

# UVM ScholarWorks

## Application Of Electrokinetics In Subsurface Energy Extraction

Item Type	dissertation;article
Authors	Peraki, Maria
Download date	2026-05-13 10:19:41
Link to Item	<a href="https://hdl.handle.net/20.500.14849/4752">https://hdl.handle.net/20.500.14849/4752</a>

APPLICATION OF ELECTROKINETICS IN SUBSURFACE ENERGY  
EXTRACTION

A Dissertation Presented

by

Maria Peraki

to

The Faculty of the Graduate College

of

The University of Vermont

In Partial Fulfillment of the Requirements  
for the Degree of Doctor of Philosophy  
Specializing in Civil and Environmental Engineering

October, 2017

Defense Date: May 15, 2017  
Dissertation Examination Committee:

Ehsan Ghazanfari, Ph.D., Advisor  
Giuseppe Petrucci, Ph.D., Chairperson  
Donna Rizzo, Ph.D.  
George Pinder, Ph.D.  
Mandar Dewoolkar, Ph.D.  
Cynthia J. Forehand, Ph.D., Dean of the Graduate College

©Copyright by  
Maria Peraki  
October, 2017

## ABSTRACT

The world's growing population results in increased energy needs that cannot yet be fully supported by the renewable sources of energy. These modern conditions and restraints have created the need to further research methods to enhance the recovery of resources previously unavailable due to technical and/or economic reasons and to reduce the environmental impacts of using fossil fuels. In this dissertation, applications of electrokinetic phenomena for the improvement of subsurface energy resource extraction are investigated using experimental and numerical tools.

Electrodialysis is proposed as a method of pre-treatment of the flow-back water produced during fracturing stage of shale gas extraction. The method targets the reduction of Total Dissolved Solids levels in the flow-back water so that it can either be treated further or be reused directly. The treatment and reuse of the flow-back water can potentially improve the sustainability of the shale gas extraction, controlling the amounts of water used and the general environmental footprint of the process.

In addition, the electrically assisted oil recovery is investigated as a potential technique for the enhancement of oil extraction, especially for the case of heavy crude oil. The high viscosity and low mobility of heavy crude oil render it almost impossible or not economical to extract. The method uses the application of low electrical field (direct current) to the oil reservoir to facilitate and increase the oil recovery by taking advantage of the mechanisms involved in electrokinetic phenomena.

## CITATIONS

Material from this dissertation has been published in the following form:

Peraki, M., Ghazanfari, E., Pinder, G.F., and Harrington, T.L.. (2016). "Electrodialysis: An Application for the Environmental Protection in Shale-gas Extraction". Separation and Purification Technology, Vol. 161, pp. 96–103.

And

Material from this dissertation has been submitted for publication to Transport in Porous Media on February 2017 in the following form:

Peraki, M., Ghazanfari, E., and Pinder, G.F.. Numerical investigation of immiscible flow for waterflooding and electrically-enhanced oil recovery.

And

Material from this dissertation has been submitted for publication to Journal of Porous Media on May 2017 in the following form:

Peraki, M., Ghazanfari, E., and Pinder, G.F.. Investigation of the feasibility of crude oil viscosity change under applied electrical field and its significance for transport phenomena.

## DEDICATION

To my sister,  
Despoina Peraki

## ACKNOWLEDGEMENTS

I would like to thank my family and Kevin Gagne for supporting me throughout writing this dissertation and my life in general. I am also grateful to Barbara Gagne, Catherine Gagne and my friends, Kate Johnson and Erica Mullane, for being my “US family”. Special thanks to my committee members for their contribution to my research and to Dr. Nikos Fytillis for his support during my first semester in UVM. I would also like to thank my many officemates through the years (Yujie, Brian, Raphael, Robert, Saleh, Zhuang, ad others) for making my office life enjoyable. Finally, I am grateful to the many Civil and Environmental Engineering undergrad students I met while being a teaching assistant for allowing me to experience the joy of teaching.

# TABLE OF CONTENTS

Citations .....	ii
Dedication .....	iii
Aknowledgements.....	iv
List of figures .....	vii
List of tables.....	ix
1. Introduction.....	1
1.1    Motivation and significance.....	1
1.1.1    Fracking, flow-back water, and issues of current water management.....	1
1.1.2    Extraction of heavy crude oil.....	3
1.2    Dissertation contributions .....	5
1.3    Research questions.....	6
1.4    Dissertation overview .....	7
2. Electrodialysis: an application for the environmental protection in the shale-gas extraction.....	8
Abstract.....	8
2.1    Introduction.....	9
2.2    Experimental program .....	14
2.2.1    Experimental set-up .....	14
2.2.2    Materials .....	15
2.2.3    Measurements .....	17
2.3    Results and discussion .....	19
2.4    Summary .....	26
3. Numerical investigation of immiscible flow for waterflooding and electrically- enhanced oil recovery .....	27
Abstract.....	27
3.1    Introduction.....	28
3.2    Methodology .....	31
3.2.1    Governing equations .....	32
3.2.1.1    Flow due to applied pressure gradient .....	32
3.2.1.2    Flow due to applied electrical gradient.....	35
3.2.2    Numerical solution scheme.....	39
3.2.3    Simulation steps.....	42
3.2.4    Numerical-experiment set-up.....	43
3.3    Results and discussion .....	48
3.3.1    Sensitivity analysis.....	49
3.3.1.1    Porosity .....	49
3.3.1.2    Relative hydraulic permeability coefficients .....	50

3.3.1.3	Absolute electro-osmotic permeability .....	51
3.3.1.4	Relative electroosmotic permeability coefficients .....	52
3.3.1.5	Initial water saturation .....	54
3.3.1.6	Oil viscosity .....	55
3.3.2	Effects of operational parameters on flow .....	56
3.3.2.1	Applied current density .....	56
3.3.2.2	Reservoir resistivity .....	57
3.3.2.3	Injection rate .....	58
3.3.3	Comparing flow in waterflooding with that of combined waterflooding and EEOR.....	59
3.4	Summary .....	60
4.	Investigation of the feasibility of crude oil viscosity change under applied electrical field in porous media and its significance for transport phenomena .....	62
	Abstract .....	62
4.1	Introduction.....	63
4.2	Physical experiment.....	67
4.2.1	Experimental set-up .....	67
4.2.2	Experimental data and results .....	71
4.3	Numerical experiment.....	75
4.3.1	Governing equations .....	75
4.3.2	Numerical experiment set-up.....	78
4.3.3	Results of numerical experiment .....	81
4.4	Summary .....	87
5.	Conclusions and future work .....	89
	Bibliography .....	93
	Appendix A: Electrodialysis data for the diluted chamber.....	102
	Appendix B: Electrodialysis data for the concentrated chamber close to the anode .....	104
	Appendix C: Electrodialysis data for the concentrated chamber close to the cathode ...	106
	Appendix D: Matlab script for numerical analysis of eeor.....	108
	Appendix E: Matlab functions for numerical analysis of eeor .....	110

## LIST OF FIGURES

Figure 2.1: Schematic of the principle of Electrodialysis (CSM: Cation Selective Membranes; ASM: Anion Selective Membranes).....	13
Figure 2.2: (a) Experimental set up, (b) Electrodialysis device.....	15
Figure 2.3: Diagrammatic representation of the factorial design .....	18
Figure 2.4: Change in TDS level in the dilute chamber for the 1-hour tests .....	23
Figure 2.5: Change in the TDS level in the dilute chamber for the 4-hour tests .....	24
Figure 2.6: Change in the TDS level in the dilute chamber for the 7-hour tests .....	25
Figure 3.1: Schematic showing field operational of combined water flooding and EEOR .....	30
Figure 3.2: Pressure distribution (in Pa) in the reservoir at: (a) 250 days, (b) 500 days, (c) 750 days, and (d) 1000 days.....	46
Figure 3.3: Voltage distribution (in V) in the reservoir at: (a) 250 days, (b) 500 days, (c) 750 days, and (d) 1000 days.....	47
Figure 3.4: Water saturation distribution at: (a) 10 days, (b) 50 days, (c) 100 days, (d) 200 days, (e) 500 days, and (f) 1000 days.....	48
Figure 4.1: Schematic showing the field operation of EEOR method.....	64
Figure 4.2: (a) Plexiglas test cell used in the experiment. The titanium electrode and the ion exchange resin beads are shown next to the cell (b) Wiring for the acquisition of voltage data (a picture of the DAQ is shown on the top center) .....	68
Figure 4.3: (a) Schematic of the experimental set-up (b) Ports used for data collection (green (1-5): voltage data collection; red (A-H): pH and ORP data collection).....	71
Figure 4.4: Voltage gradient at the center of the cell (Ports 3 and 4).....	72
Figure 4.5: Measured pH at: (a) the ports closer to the anode and (b) the ports closer to the cathode. $x$ is the distance from the anode and $L$ the total length of the cell (60 cm).....	73
Figure 4.6: Schematic of the 2D reservoir used in simulation.....	79
Figure 4.7: Results of numerical simulation for cumulative oil production for different values of oil viscosity.....	80
Figure 4. 8: Results of numerical simulation using experimental data presented in Section 4.2. The applied current density is $0.1 \text{ A/m}^2$ and the initial oil viscosity is 2,810 cp.....	82
Figure 4.9: Results of numerical simulation using experimental data from Ghazanfari, 2013 (light crude oil). The applied current density is $0.78 \text{ A/m}^2$ and the initial oil viscosity is 97 cp.....	84

Figure 4.10: Results of numerical simulation using experimental data from Wittle et al., 2009. The applied current density is $1 \text{ A/m}^2$ and the initial oil viscosity is 2,635 cp.....	85
Figure 4.11: Results of numerical simulation using field data from Golfo San Jorge Basin (Hill, 2014). The applied current density is $1 \text{ A/m}^2$ and the initial oil viscosity is 2,854 cp.....	87

## LIST OF TABLES

Table 2.1: Properties of the ion selective membranes (as given by the manufacturer) ....	16
Table 2.2: Information of tests.....	18
Table 2.3: Least Mean Squares Contrast ( $\alpha=0.05$ ) .....	20
Table 2.4: Factorial Analysis ( $\alpha=0.05$ ).....	20
Table 2.5: Least Squares Means Differences by Tukey for the duration of the test ( $\alpha=0.05$ ) .....	21
Table 2.6: Measurements of temperature and pH from the dilute chamber for selected tests .....	22
Table 3.1: Characteristics of reservoir used in numerical simulation.....	44
Table 4.1: Physical properties of the ion exchange resins used for pH control.....	70
Table 4.2: Characteristics of reservoir used in numerical simulation.....	79

# CHAPTER 1

## INTRODUCTION

### 1.1 MOTIVATION AND SIGNIFICANCE

This dissertation constitutes an effort to advance and improve the operation of subsurface resource extraction. The first part of this dissertation, investigates the efficiency of the electrodialysis for desalination of flow-back water at the laboratory scale using samples of flow-back water from the Marcellus shale-gas formation. After performing preliminary tests to examine the applicability of the method, a series of trials were conducted. The trials were designed in a way that allowed the use of factorial analysis to study the variance of the experimental data and outline the most important variables of the method. The second part of the dissertation uses experimental and numerical tools to investigate the mechanisms of an applied electric field on oil reservoirs for oil recovery and their contribution to the flow during oil recovery. The examined method is called Electrically Enhanced Oil Recovery (EEOR).

#### 1.1.1 FRACKING, FLOW-BACK WATER, AND ISSUES OF CURRENT WATER MANAGEMENT

Shale formations have extremely low permeability, which makes hydraulic fracturing (fracking) a required process for economically viable shale gas extraction (Hayes, 2012). The process involves the injection of the fracking fluid at high pressure into the formation. The main supplies of water for hydraulic fracturing are surface water,

ground water, and recycled water (Arthur, 2011). The volume of the injected fracking fluid, a combination of water and various chemical additives, varies among different shale gas formations and even among the wells of the same shale gas formation (Arthur, 2011). In Marcellus shale, only 10-20% of the injected volume is recovered as a wastewater stream, known as flow-back water, while the rest of it remains bound to the dry shale matrix (Abdalla et al., 2011; Arthur, 2011; Rahm et al., 2013; Veil, 2010).

Flow-back water is a mixture of fracking fluids returning to the surface and chemical constituents originating from the shale formation (Arthur, 2011; Rahm et al., 2013). The predominant constituents of flow-back water are the dissolved salts (Haluszczak et al., 2012). The dissolved salts can be identified using conductivity, salinity, or total dissolved solids (TDS) measurements. (Arthur, 2011; Castle et al., 2013; Hayes, 2012; Lutz and Lewis, 2013). The most common compounds of TDS are calcium, magnesium, chloride, sodium, sulfate, barium and iron (Arthur, 2011; Castle et al., 2013; Haluszczak et al., 2012; Hayes, 2012). The flow-back water also contains chemical additives used during the drilling, fracturing, and operation of the well and in some cases naturally occurring radioactive materials (Arthur, 2011; Castle et al., 2013; Hayes, 2012).

With high production rates in the USA, flow-back water is the largest byproduct stream of shale-gas extraction (Arthur, 2011). The high salinity requires proper management of the flow-back water (Haluszczak et al., 2012).

The common practice in shale-gas extraction for the management of flow-back water is the disposal in deep wells (Class II wells). However, after earthquake incidents in the state of Ohio that are linked with the injection of waste water in deep wells and the

environmental indicators of elevated TDS have been noted in the Monongahela River (Pennsylvania and West Virginia), including elevated concentrations of chloride and golden algal blooms that produce toxins that can suffocate aquatic organisms, the need for treatment and recycling of the flow-back water has become more apparent (Haluszczak et al., 2012; Lutz and Lewis, 2013).

Incidents like the above-mentioned render the treatment of the flow-back water vital for the protection of the public and of the environment. The industry standard for acceptable recycle water TDS level, is a maximum of 50,000 mg/L (Ziewkiewicz et al., 2012). However, limits for acceptable reuse may vary widely depending on the driller. In some cases water with a TDS level greater than 50,000 mg/l has been used as recycle water (Ziewkiewicz et al., 2012).

Most companies apply a basic settling and filtration treatment of the flow-back water, which is subsequently mixed with fresh water in order to reduce the TDS levels so that it can be reused for other fracturing jobs. However, this method requires the use of additional fresh water (Arthur, 2011; Veil, 2010). The shale-gas industry is in search of alternative efficient and economical remediation technologies (Veil, 2010). The efficiency of the electrodialysis for desalination of flow-back water as a pre-treatment option is investigated in this dissertation.

### 1.1.2 EXTRACTION OF HEAVY CRUDE OIL

Oil recovery vice the natural forces of the reservoir is called primary recovery phase (Morris, et al., 1985). As oil moves toward the surface and gets extracted, the pressure of

the reservoir drops resulting in a lack of sufficient natural drive (Latil, 1980; Morris, et al., 1985). Methods to enhance the extraction of oil implemented early in the production of the reservoir are called secondary stage oil recovery methods (Latil, 1980). This stage involves the injection of water or gas into the reservoir to increase the pressure and enhance the natural flow of oil toward lower pressure at the surface (Morris, et al., 1985).

If the reservoir holds sufficient amounts of oil toward the end of the secondary stage which can be economically extracted, then tertiary methods of enhancement may be employed. These secondary and tertiary stage extraction activities are usually called enhanced oil recovery methods (EOR) (Latil, 1980; Morris, et al., 1985).

Waterflooding is the most commonly used method of enhanced oil recovery (Latil, 1980). The method belongs to the secondary stage of oil recovery (Latil, 1980; Greenkorn, 1983) and is applied for the enhancement of the drive mechanism (pressure) that facilitates the oil production (Morris, et al., 1985). Water is injected into the reservoir via an injection well. The injection of water serves a dual purpose; it displaces the oil through the pores moving it toward the production wells while it increases the reservoir pressure, which also enhances the movement of oil toward the production well (Latil, 1980).

The easily extracted oil deposits have mostly been discovered and will be depleted soon. The viscosity of heavy crude oil usually ranges between 100 and 10000 cp and combined with its low mobility ratios, makes the extraction of heavy crude oil impossible even for the enhanced oil recovery methods. The traditional EOR methods are usually either insufficient, or economically inefficient, or even harmful to the environment. Thus,

it is necessary to develop and implement new methods that will overcome these obstacles (Okandan, 1982).

Electrically Enhanced Oil Recovery (EEOR) is a new method that takes advantage of electrokinetic phenomena for oil production. This dissertation presents an experimental and numerical investigation of the EEOR method in an attempt to provide insight into the feasibility and the important parameters involved in the method.

## 1.2 DISSERTATION CONTRIBUTIONS

The first part of this dissertation contributes to the advancement of knowledge in application of electrodialysis for the pre-treatment of flow-back water produced from shale gas industry. The effectiveness of the technique for TDS removal was extensively investigated and resulted in unique experimental dataset. The second part of the dissertation advances the knowledge on the transport phenomena during EEOR method using experimental and numerical tools.

The dissertation will benefit society by improving the understanding of the methods capable of reducing the environmental impacts involved in subsurface energy extraction, particularly shale gas and enhanced oil recovery. Both methods intend to improve the process of fossil fuels extraction, which remains the main source of energy, and to reduce the oil and gas industry's footprint on the environment. Electrodialysis intends to conserve available water supplies and to minimize the waste disposal by enabling flow-back water reuse during the fracturing of shale formations, while EEOR aims at increasing the heavy crude oil recovery through a process that does not add significant stresses on the

environment (e.g. no additional water usage, no hazardous chemicals, no drilling). EEOR method contributes to meeting the energy demands, and smooth transition to a “clean” energy production in future.

### 1.3 RESEARCH QUESTIONS

The research questions that were addressed in this dissertation are divided into two parts: the first part refers to the electrodialysis treatment of flow-back water and the second part refers to the electrically enhanced oil recovery. For the first part, the research questions are:

- o Is electrodialysis an efficient pre-treatment method for the TDS removal from flow-back water sample?
- o Which parameters significantly affect the TDS removal, and hence, mainly controls the method’s efficiency?

For the second part, the research questions include:

- o Does the combination of EEOR and waterflooding significantly increase oil recovery? Which parameters mainly control the transport phenomena during the application of the method?
- o Does EEOR method induce electro-chemical reactions that reduce the viscosity of crude oil? If yes, how important is the effect of the reduced crude oil viscosity on oil recovery transport phenomena?

## 1.4 DISSERTATION OVERVIEW

The dissertation is organized as follows:

- Chapter 2: The efficiency of the electrodialysis for desalination of flow-back water was investigated at the laboratory scale using samples of flow-back water from the Marcellus shale-gas formation. To facilitate the analysis of the experimental data, a factorial statistical design was employed. The results of the factorial analysis, were used to identify the parameter that significantly affects the efficiency of the method.
- Chapter 3: A numerical investigation of the EEOR method was performed in an attempt to provide insight into the importance of the parameters involved in the method. A sensitivity analysis was performed on important reservoir and operational parameters involved in the combined waterflooding and EEOR method.
- Chapter 4: The feasibility of oil viscosity change due to an applied electrical field and its importance in transport phenomena during oil recovery was investigated using experimental and numerical tools. The physical experiment simulated the application of an applied electrical field to a synthetic formation in a small-scale test cell. To examine the effect of the change in oil viscosity on transport, and therefore on oil production, a numerical experiment was performed.

## CHAPTER 2

# ELECTRODIALYSIS: AN APPLICATION FOR THE ENVIRONMENTAL PROTECTION IN THE SHALE-GAS EXTRACTION

### ABSTRACT

Water is one of the resources used to fracture the host formation and retrieve the trapped gas during the process of shale-gas extraction. A portion of the injected water, which is known as flow-back water, is recovered during the initial extraction of the gas. The main characteristic of flow-back water is the very high concentrations of dissolved solids (e.g. calcium, sodium, and chloride), which renders its treatment highly challenging for most existing treatment methods. An alternative for onsite treatment (or pre-treatment) and recycling of the flow-back water is electro dialysis. The method is based on an electrically assisted membrane process for separation of salts from the solution. In this chapter, the efficiency of the electro dialysis for desalination of flow-back water was investigated at the laboratory scale using samples of flow-back water from the Marcellus shale-gas formation.

## 2.1 INTRODUCTION

Shale formations are known to have extremely low permeability, which makes hydraulic fracturing (fracking) a required process for economically viable shale gas extraction (Hayes, 2012). The process consists of the injection of the fracking fluid at high pressure into the formation. The fracking fluid is a combination of water and various chemical additives (Arthur, 2011). The volume of the injected fracking fluid varies among different shale gas formations and even among the wells of the same shale gas formation. In the Marcellus formation, the volume of injected fracking fluid ranges between 10,000 and 30,000 cubic meters per well (Abdalla et al., 2011; Rahm et al., 2013). Almost 90% of the injected volume remains bound to the dry shale matrix and only 10-20% is recovered as a wastewater stream, known as flow-back water (Abdalla et al., 2011; Arthur, 2011; Rahm et al., 2013; Veil, 2010). The main supplies of water for hydraulic fracturing are surface water, ground water, and recycled water (Arthur, 2011).

Flow-back water is considered as a mixture of fracking fluids returning to the surface and chemical constituents originating from the shale formation (Arthur, 2011; Rahm et al., 2013). The predominant constituents of flow-back water are the dissolved salts (Haluszczak et al., 2012). The dissolved salts can be identified using conductivity, salinity, or total dissolved solids (TDS) measurements. The concentration of Total Dissolved Solids (TDS) in the flow-back water of the Marcellus formation varies between 30,000 mg/L and 200,000 mg/L (Arthur, 2011; Castle et al., 2013; Hayes, 2012; Lutz and Lewis, 2013). The most common compounds of TDS are calcium, magnesium, chloride, sodium, sulfate, barium and iron (Arthur, 2011; Castle et al., 2013; Haluszczak et al., 2012; Hayes, 2012).

The flow-back also contains chemical additives used during the drilling, fracturing, and operation of the well and in some cases naturally occurring radioactive materials (Arthur, 2011; Castle et al., 2013; Hayes, 2012). With a production of about 21 billion barrels per year (2011) in the USA, flow-back water is the largest byproduct stream of shale-gas extraction (Arthur, 2011). The high salinity requires proper management of the flow-back water (Haluszczak et al., 2012). In Marcellus, the gas industry drilled 1,386 Marcellus wells in 2010, compared to 763 in 2009. From 2012 to 2013, 2,013 permits were issued and 1,074 wells were drilled. Therefore, the water demand, and consequently, the volume of the wastewater stream has increased significantly in recent years (Abdalla et al., 2011; Rahm et al., 2013). Although, the development operations in the Marcellus have access to sufficient water supplies, the treatment and disposal of the flow-back water represent a major cost item (Godec et al., 2007; Hayes, 2012; Veil, 2010).

The common practice in shale-gas extraction for the management of flow-back water is the disposal in deep wells (Class II wells). In the Marcellus, there are only 8 Class II wells for this purpose (Hayes, 2012). In 2013 in Pennsylvania, about 87 % of the flow-back water was transported to commercial wastewater treatment plants that operate under the supervision of the state environmental protection agency (Arthur, 2011; Hayes, 2012; Lutz and Lewis, 2013; Veil, 2010). However, after the recent earthquakes in the state of Ohio that are linked with the injection of waste water in deep wells and the recent environmental indicators of elevated TDS have been noted in the Monongahela River (Pennsylvania and West Virginia), including elevated concentrations of chloride and golden algal blooms that produce toxins that can suffocate aquatic organisms, the need for treatment and recycling of the flow-back water has become more apparent (Haluszczak et

al., 2012; Lutz and Lewis, 2013). A step forward has been made on this direction as the amount of flow-back water that is recycled has increased from 11% prior 2011 to 56% in 2011 (Lutz and Lewis, 2013), while Shale Media Group reported that the amount increased to 90% by 2015.

Incidents like the above-mentioned render the treatment of the flow-back water vital for the protection of the public and of the environment. The industry standard for acceptable recycle water TDS level, is a maximum of 50,000 mg/L (Ziewkiewicz et al., 2012). However, limits for acceptable reuse may vary widely depending on the driller. In some cases, water with a TDS level greater than 50,000 mg/l has been used as recycle water (Ziewkiewicz et al., 2012). Most companies apply a basic settling and filtration treatment of the flow-back water, which is subsequently mixed with fresh water in order to reduce the TDS levels so that it can be reused for other fracturing jobs. However, this method requires the use of additional fresh water (Arthur, 2011; Veil, 2010). Since May 2010, the state of Pennsylvania has established more stringent discharge requirements for the TDS concentrations and the shale-gas industry is in search of alternative efficient and economical remediation technologies (Veil, 2010). The efficiency of the electro dialysis for desalination of flow-back water is investigated.

Electrodialysis was first proposed in 1890 by Maigrot and Sabates for demineralization of sugar syrup (Maigrot and Sabates, 1890). Electrodialysis has been used for over 50 years for desalination of brackish water, seawater and industrial water Bishop and Murphy, 1972; Pilat, 2001; Turek, 2002; Mohammadi and Kaviani, 2003; Sadrzadeh and Mohammadi, 2008, 2009; Tanaka, 2012; Ghyselbrecht et al., 2013). It is also used in

the food industry for purification, modification, or concentration of food (Basinet et al., 1998), and recently for the production of organic acids (Huang et. al, 2007). The method is an electrochemical process in which the ions are transferred through ion-selective membranes from one solution to another using a low Direct Current (DC) electric field as the driving force (Sadrzadeh et al., 2007; Ghyselbrecht et al., 2013). Two different outflows are produced in the process, the dilute flow with lower TDS level than the inflow, and the concentrated flow with higher TDS level than the inflow (Sonune and Ghate, 2004; Banasiak et al., 2007; Strathmann, 2010; Hayes, 2012; Ghyselbrecht et al., 2013). Figure 2.1 is a schematic showing the operating principle of electrodialysis. The performance of the electrodialysis method depends on various parameters such as the applied voltage, the flow rate, the properties of the membranes, the composition of the inflow, and the design parameters of the equipment (e.g. stack construction, cell dimensions, etc.) (Lee et al., 2002; Banasiak et al., 2007; Sadrzadeh et al., 2007; Sadrzadeh and Mohammadi, 2008, 2009). The main investment cost of the method is that associated with the membranes, which depends on the required membrane area. The cost of operation is mainly determined by the energy requirements for the application of the DC electric field (Lee et al., 2002).

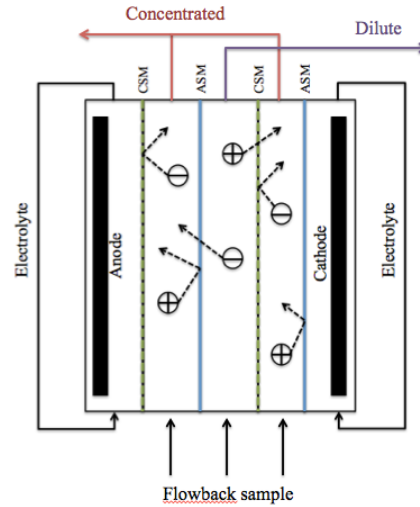


Figure 2.1: Schematic of the principle of Electrodialysis (CSM: Cation Selective Membranes; ASM: Anion Selective Membranes)

Ion selective membranes are made of a macromolecular material having ionizable groups such as ion-exchange resins (Bazinet et al., 1998). The ion selective membranes are basically ion exchange resins in the form of a film. They have evolved from a laboratory tool to an industrial product (Xu, 2005; Kariduraganavar et al., 2006; Strathmann, 2010). The two main categories are the cation and the anion selective membranes. The cation selective membranes include negatively charged groups (e.g.  $-\text{SO}_3^-$ ,  $-\text{COO}^-$ ,  $-\text{PO}_3^{2-}$ ) that only allow the movement of the cations. In contrast, the anion selective membranes allow the movement of the anions using positively charged groups (e.g.  $-\text{NH}_3^+$ ,  $-\text{NRH}^{2+}$ ,  $\text{PR}^{3+}$ ). The desired properties of the ion selective membranes are high permselectivity; low electrical resistance; high mechanical, thermal, and chemical stability; and low cost of production (Xu, 2005; Kariduraganavar et al., 2006; Strathmann, 2010).

This chapter investigates the efficiency of electro dialysis as a desalination process (pre-treatment) at the laboratory scale for flow-back water samples taken from Marcellus shale wells.

## 2.2 EXPERIMENTAL PROGRAM

### 3.2.1 EXPERIMENTAL SET-UP

The experimental set up used in this chapter is shown in

Figure 2.2(a). It consisted of the electro dialysis device, the peristaltic pump, the power supply for application of the DC electric field, and the container for the electrolyte. The design of the device was based on the principle of electro dialysis, as shown in Figure 2.1. Three pairs of anion and cation selective membranes were used within the device. The role of the central pair of membranes was to trap the anions and the cations of the feed (flow-back water) in the concentrated chambers. The two external pairs of membranes were used to separate the electrolyte from the feed.

The device consisted of five chambers including two electrode chambers, two chambers for the concentrated outflow, and one chamber for the dilute outflow, as shown in

Figure 2.2(b). The chambers were made of propylene to prevent reactions caused by application of the electrical field. The dimensions of the device were 30cm x 9cm x 9cm. For the tests that used sodium sulfate ( $\text{Na}_2\text{SO}_4$ ) as the electrolyte, titanium electrodes were placed in the chambers using four titanium bolts that were also used for the connection

of the electrodes to the power supply. However, electrodes made of graphite were used for the tests using sodium chloride (NaCl) as the electrolyte, due to the corrosion that the NaCl caused to the titanium electrodes. Bolts that penetrated the frame of all the chambers were placed in the perimeter to keep the device sealed and to prevent leakage. A peristaltic pump was used for injection of the feed to the three central chambers and then, for circulation of the electrolyte within the electrodes chambers. Flow only existed in the electrode chambers and no circulation was used for the central chambers (batch system). As shown in

Figure 2.2 (a), the device was placed in a vertical position to facilitate the injection from the bottom ports of the device and to remove existing air in the chambers from the top ports. A power supply was used to apply the electric field through the electrodes.

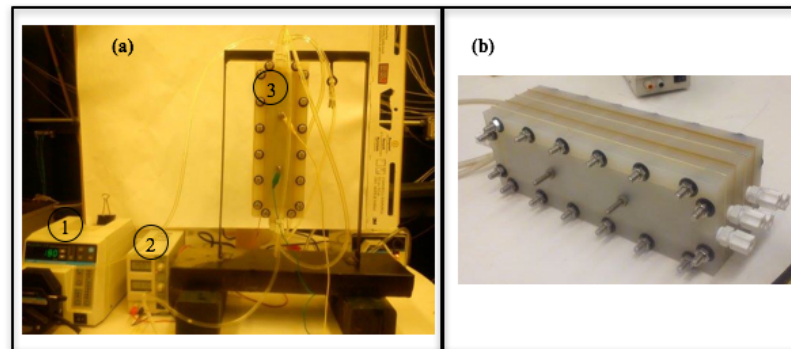


Figure 2.2: (a) Experimental set up (1: Peristaltic pump; 2: Power supply; 3: Electro dialysis device), (b) Electro dialysis device

### 3.2.2 MATERIALS

The flow-back samples were obtained from Marcellus wells located in the Washington County, Pennsylvania. The initial TDS levels of flow-back samples were measured at approximately 100,000 mg/L. During some tests, the initial concentration was

near 60,000 mg/L due to the dilution of the samples in order to evaluate the influence of the initial concentration. ICP (Inductively Coupled Plasma) analysis was run on samples of previous experiments and it was concluded that calcium, sodium and chloride are the main elements contained in the flow-back samples that were used. Properties of the anion and cation selective membranes are listed in Table 2.1.

Two different electrolyte solutions were used in the experiments including: (i) a brine solution with a concentration of 90 g/L  $\text{Na}_2\text{SO}_4$  (2 rounds-18 tests) and 125 g/L  $\text{Na}_2\text{SO}_4$  (1 round-9 tests), and (ii) a solution of 90 g/L  $\text{NaCl}$  (1 round-9 tests). Although, using  $\text{NaCl}$  solution as the electrolyte resulted in reduction of the TDS level of more than 90% (Peraki et al., 2014), it caused massive corrosion of the titanium electrodes. A system of two different electrolytes for each electrode chamber ( $\text{NaCl}$  for the cathode and  $\text{Na}_2\text{SO}_4$  for the anode) was also used, but the reduction of TDS level was insignificant.

Table 2.1: Properties of the ion selective membranes (as given by the manufacturer)

<b>Property</b>	<b>Anion selective membrane</b>	<b>Cation selective membrane</b>
Technical Specification	AMI-7001S	CMI-7000S
Functionality	Strong Base Anion Exchange Membrane	Strong Acid Cation Exchange membrane
Polymer Structure	Gel polystyrene cross linked with divinylbenzene	Gel polystyrene cross linked with divinylbenzene
Functional Group	Quaternary Ammonium	Sulphonic Acid
Standard thickness (mm)	0.45	0.45
Chemical Stability Range (pH)	1-10	1-10

### 3.2.3 MEASUREMENTS

To facilitate the analysis of the experimental data, a factorial statistical design was employed. A factor is a kind of treatment and, in this particular set of experiments, the two selected factors were the duration of the application of the electric field and the current. The dependent parameter was the change in TDS level (%) for the dilute chamber. The reason for the selection of these factors was that they mainly control the cost of the method. Three levels of each factor were considered for each of the two electrolytes. Twenty seven tests (divided into 3 rounds) were conducted using the one type of electrolyte ( $\text{Na}_2\text{SO}_4$ ), and 9 tests (1 round) using the second electrolyte ( $\text{NaCl}$ ). The factorial design used for the analysis of the experimental data is shown in Figure 2.3. Along the x axis are plotted the three values of duration in hours (level 2), along the y axis the applied current in Amps (level 1), and along the z axis the number of the round. Each block in this figure represents a test. Thus, for example, block “a” denotes a test of round 1 using 2 A of current applied for 1 hour. Block “b” also represents a test of round 1, however, the applied current is 1 A and the duration is 4 hours. Table 2.2 summarizes the information of each test. Three different values of applied current and time duration were selected. For each of the two factors a low, medium, and high value were selected. The maximum values for each factor were selected in a way that will control the maximum cost of the application and maintain it in a considerably low level. Each of the nine trials of each round consisted a different combination of the selected values. The TDS level, conductivity and occasionally the temperature, and the pH were measured during the experiments. For the TDS level analysis, the standard method (ASTM D5907) was followed. Readings of the current and

the voltage between the top and the bottom bolts connected to the electrodes were taken during the experiments. The results of these experiments are presented in the following section.

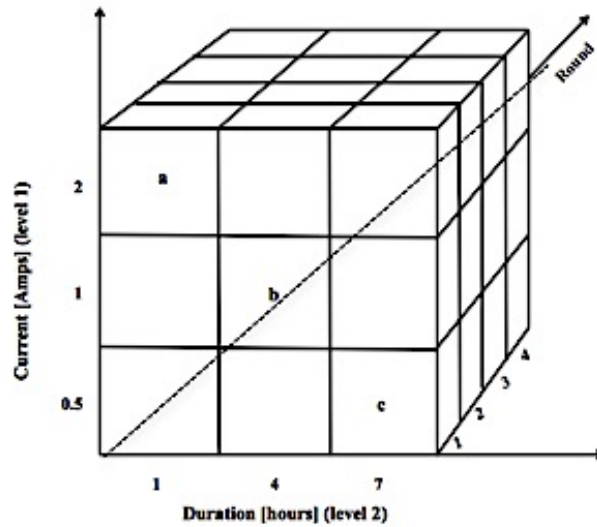


Figure 2.3: Diagrammatic representation of the factorial design

Table 2.2: Information of tests

Test	Electrolyte	Initial concentration of the flow-back sample (mg/L)
Round 1 (ED1-1 through ED1-9)	Sodium sulfate (90g/L)	~100,000
Round 2 (ED2-1 through ED2-9)	Sodium sulfate (90g/L)	~100,000
Round 3 (ED3-1 through ED3-9)	Sodium sulfate (125 g/L)	~ 65,000
Round 4 (ED4-1 through ED4-9)	Sodium chloride (90 g/L)	~ 65,000

## 2.3 RESULTS AND DISCUSSION

The experimental program was designed according to the factorial analysis, a method of analyzing variance. In order to properly use this method, all the initial parameters of the experiments have to be the same among the tests except the parameters that were set as factors, in this case the current and the duration of the experiment. Table 2.2 contains all the information on the initial parameters among the tests. Note that Rounds 1 and 2 are identical. Rounds 3 and 4 vary from Rounds 1 and 2 based upon the concentration of the electrolyte (Round 2), the type of the electrolyte (Round 3), and the range of the initial concentration of the sample (Rounds 3 and 4).

In order to be able to use all the rounds for the factorial analysis, an additional analysis of variance was performed among the rounds using the software JMP Pro 11. The TDS levels of the two identical rounds were compared to the remaining two in order to determine if the difference in the above-mentioned parameters (range of initial concentration of the sample, type and concentration of electrolyte) are statistically significant in terms of change in TDS level.

The analysis used is called Least Mean Squares Contrast. A contrast is a set of linear combinations of parameters that one wants to jointly test to be zero. Alpha ( $\alpha$ ), a parameter that denotes the significance level of the test, was set to be 0.05 (95% certainty) and it was compared to the resulted p-value of the analysis. Table 2.3 shows the results of the analysis of variance. For all the comparisons, the p-value was greater than 0.05, so the values of the dependent variable do not present a statistically significant difference depending on the round meaning that Rounds 1, 2, 3, and 4 can be used for the factorial analysis.

Table 2.3: Least Mean Squares Contrast ( $\alpha=0.05$ )

<b>Test Detail</b>		
<b>Comparison</b>	<b>Parameter</b>	<b>Value</b>
Rounds 1, 2 compared to round 3	F Ratio	0.2381
	p-value (F-test)	0.6289
Rounds 1, 2 compared to round 4	F Ratio	0.7212
	p-value (F-test)	0.4021
Round 3 compared to round 4	F Ratio	1.3410
	p-value (F-test)	0.2554

The factorial analysis was performed using the data of all 36 tests as input. Table 2.4 contains the results of the factorial analysis. The calculated p-values for the current and the cross-correlation of the current and the duration, were greater than alpha ( $\alpha=0.05$ ) meaning that the two parameters do not result in statistically significant difference in the values of the change in TDS level at the 95% confidence level. However, the duration of the test was calculated to be very nearly significant at the 95% confidence level. The interpretation of this result is that the duration of the experiment is the parameter that results in changes in the TDS level that are statistically significant.

Table 2.4: Factorial Analysis ( $\alpha=0.05$ )

<b>Effect tests</b>		
<b>Source</b>	<b>F Ratio</b>	<b>p-value</b>
Current (A)	0.4076	0.6693
Duration (hr)	3.3211	0.0513
Current (A)*Duration (hr)	0.4555	0.7676

In order to support the assumption that the TDS levels corresponding to the different values of duration can be considered statistically significant, the Least Square Difference Method by Tukey was performed on the three duration values. Table 2.5 presents the results corresponding to the duration as this was the only case with statistically significant difference among the values of the change in TDS level due to the value of the factor. Levels not connected by the same letter are significantly different. As is shown in Table 2.5, the results between the 1-hour tests and the 7-hour test are the ones that differ significantly. However, the results of the intermediate value of 4 hours were not considered to vary significantly in comparison with the 1-hour or the 7-hour tests.

Table 2.5: Least Squares Means Differences by Tukey for the duration of the test ( $\alpha=0.05$ )

Level		
1-hr	A	
4-hr	A	B
7-hr		B

The most important result of the statistical analysis was not the effect of the time duration but the insignificant effect (in statistical terms) of the applied current's magnitude. This indicates that a long duration in combination with an intermediate current can produce a high reduction in the TDS level. Based on this, the results of the change in TDS level for the dilute chamber were divided into different graphs depending on the duration of the test (Figure 2.4 Figure 2.6). The complete dataset and the results for the two concentrated chambers are presented in the Appendices A, B and C.

Measurements of conductivity for the dilute chamber are also included in Appendix A. Due to the close relationship between the conductivity and the TDS level, the conductivity was used as a preliminary indicator of the performance of the method.

Table 2.6 summarizes the measurement of pH and temperature at the beginning and at the end of selected tests. The values of these two parameters did not change significantly so their impact on the process was not considered significant. However, different initial values of those parameters could potentially affect the results of the process.

Table 2.6: Measurements of temperature and pH from the dilute chamber for selected tests

<b>Test</b>	<b>Initial pH</b>	<b>Final pH</b>	<b>Initial Temperature (°F)</b>	<b>Final Temperature (°F)</b>
ED2-6	9.41	9.46	-	-
ED2-9	9.41	8.50	-	-
ED3-1	-	-	57	59
ED3-2	-	-	59	59
ED3-3	9.25	9.16	60	59
ED3-4	-	-	57	60
ED3-5	-	-	59	59
ED3-6	9.25	9.16	59	60
ED3-7	-	-	57	59
ED3-8	-	-	59	60
ED3-9	9.25	9.16	59	60

The main focus of this chapter is the dilute chamber's behavior and therefore, the results for this particular chamber are presented in detail in the following section.

Figure 2.4 presents the results corresponding to the 1-hour tests for all four rounds. As it can be seen, during all four rounds the TDS level was reduced except in the cases of two tests during Round 2. The roll from which the membranes for Round 1 were cut was

almost a year old; however, a new roll was used for the rest of the rounds. The age of the membranes in the beginning of the round might have had an effect on the permselectivity of the membranes, especially in the case where the duration of each test was only one hour. It is interesting to note that even in the case of the highest applied current (2 A), there was an increase in the TDS concentration for round 1 as the duration of the test was not long enough. The 1-hour tests seemed to be dominated by the phenomenon of diffusion due to the difference in the concentration among the chambers especially in the case when only 0.5 A were applied. This may imply that the results of the 1-hour tests are the least representative of the method.

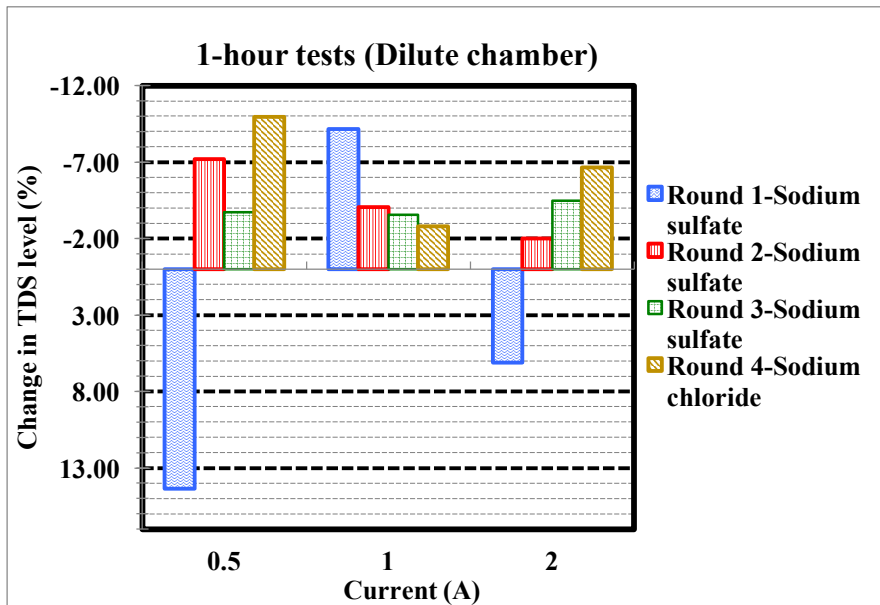


Figure 2.4: Change in TDS level in the dilute chamber for the 1-hour tests

Figure 2.5 presents the results corresponding to the 4-hour tests for all four rounds. Similarly to the data in Figure 2.4, there was an increase in the TDS level for Round 1, however, only for one test. This fact further supports the finding that duration causes a

statically significant change in the resulting TDS level and that it is the defining parameter in the method. The increase in the duration resulted in more consistent results, with Round 4 having the highest reduction in TDS level for an applied current of 2 A.

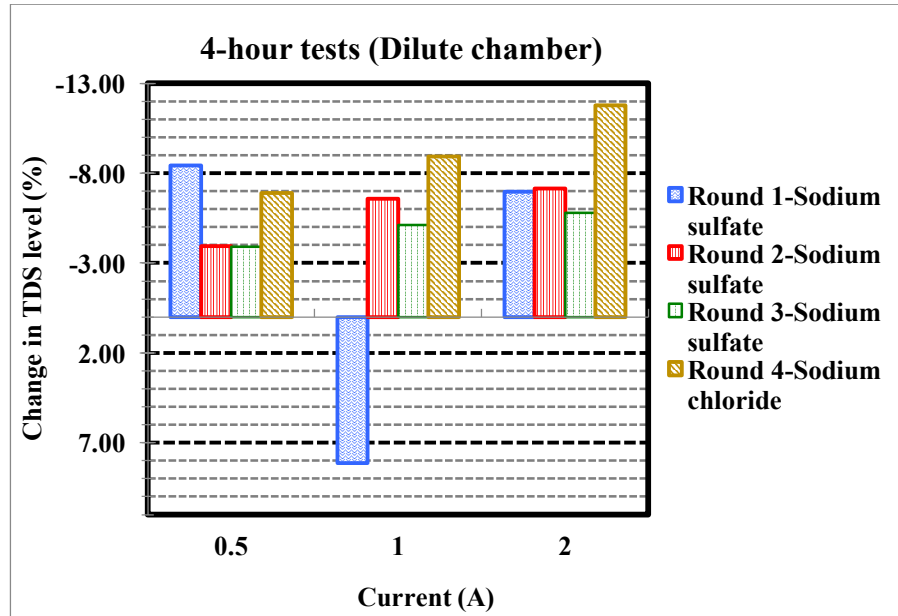


Figure 2.5: Change in the TDS level in the dilute chamber for the 4-hour tests

Figure 2.6 presents the results corresponding to the 7-hour tests for all four rounds. Contrary to the previous data, there was no increase in the TDS level for any experiment. This fact adds to the finding that the increase of the duration resulted in more consistent results. Round 1 had the highest reduction in TDS level, although the roll used for the membranes was older. These results may be attributed to the fact that as time passes chemical reactions are taking place in the reservoir where the sample is stored, causing some minor changes to the concentration of the various chemical compounds. A supporting evidence of this supposition is the fact that a white layer of salt was discovered on the

bottom of the middle chambers at the end of each test. The film was removed each time, but its thickness was increasing as the time was passing.

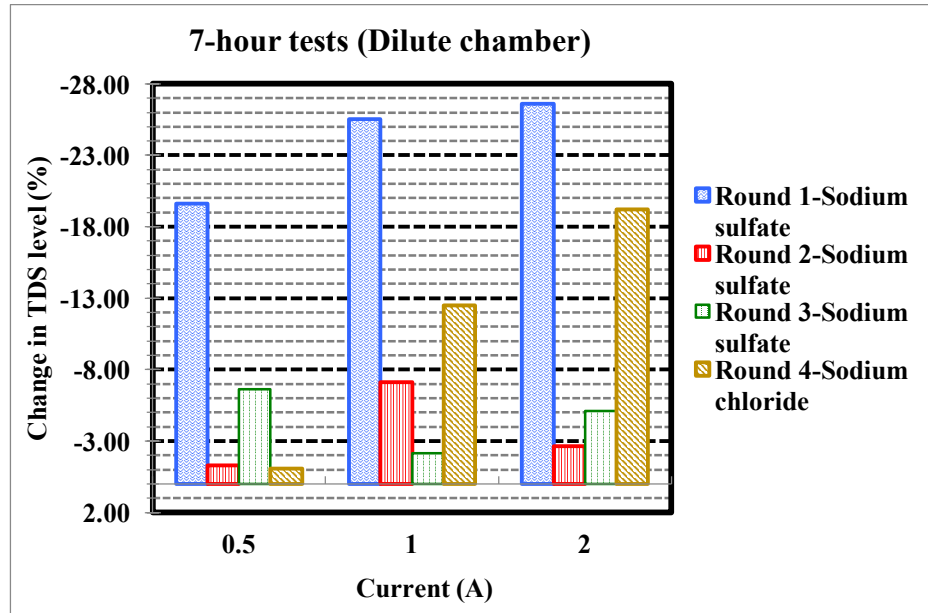


Figure 2.6: Change in the TDS level in the dilute chamber for the 7-hour tests

Overall, the duration proved to be the most important parameter in order to obtain the most consistent results. Any increase in the TDS level was eliminated as the duration of the test increased. Sodium chloride seemed to perform more steadily than sodium sulfate despite the fact that it didn't result in a higher reduction for all the tests. The more consistent performance may be attributed to the fact that the flow-back sample already contained sodium and chloride, but it did not contain sulfate. This may have caused some additional chemical reactions, especially in the concentrated chambers that were located close to the electrode chambers. The data from the two concentrated chambers are presented in the Appendices B and C. Some cases of a decrease of TDS level were noted, although the TDS

level was supposed to increase after the test. Round 4 is the one that had the least incidents of decrease in the concentrated chambers, proving that sodium chloride performed better as an electrolyte.

## 2.4 SUMMARY

Efficiency of electro dialysis as a pre-treatment option for flow-back water from shale gas wells was investigated through laboratory scale experiments. Electro dialysis was found to be a relatively effective method for TDS level reduction for flow-back water. Using  $\text{Na}_2\text{SO}_4$  or  $\text{NaCl}$  solution as electrolyte, the maximum TDS level reduction was found to be about 27% after 7 hours of low direct current electric field application. The parameter that affects the results the most was found to be the duration of the test. The applied current seemed to perform a secondary role. However, an intermediate value of applied current is a better choice to overcome the effect of the diffusion of the ions through the membranes. The type of the electrolyte, the concentration of the electrolyte and the range of the initial concentration did not cause a statistically significant difference in the results. However,  $\text{NaCl}$  as an electrolyte presented a steadier and more consistent performance than  $\text{Na}_2\text{SO}_4$ .

## CHAPTER 3

# NUMERICAL INVESTIGATION OF IMMISCIBLE FLOW FOR WATERFLOODING AND ELECTRICALLY-ENHANCED OIL RECOVERY

### ABSTRACT

The study of two-phase immiscible flow in porous media using electrokinetics is important in different fields including the remediation of hydrocarbon contaminated soils and enhanced oil recovery. While electrokinetic technology has been used for treatment and decontamination of hydrocarbon polluted sites, electrically enhanced oil recovery (EEOR) is relatively new. Although a few laboratory and field experiments have investigated the potential promise of the EEOR method, further investigation is necessary to better understand the fundamentals and the importance of different parameters/processes involved in the method. This chapter presents a numerical investigation of the EEOR method in an attempt to provide insight into the feasibility of, and the important parameters involved in the method. A sensitivity analysis was performed on important reservoir and operational parameters involved in the combined waterflooding and EEOR method. Most of the investigated reservoir and operational parameters were found to be significant and critical to the transport phenomena controlling the oil production. In addition, the results showed that the applied electrical gradient involved in EEOR combined with the waterflooding method contributed to a very small increase in oil production.

### 3.1 INTRODUCTION

Knowledge of transport phenomena in porous media is essential in several disciplines (Scheidegger, 1957; Chavent and Jeffre, 1986; Civan, 2011) including soil science, groundwater hydrology, petroleum engineering, storage of energy byproducts in deep geological formations, and biomedical engineering among others (Greenkorn, 1983; Weir et al., 1996; Khaled and Vafai, 2003; Pinder and Gray, 2008; Kim et al., 2014).

A sub-problem of transport in porous media is two-phase immiscible flow in geological formations. It is important to understand and predict the behavior as it is significant in the remediation of hydrocarbon polluted sites (Hunter, 1981; Bruell et al., 1992, Wise, 2000) and in oil recovery (Amba et al., 1964; Haroun et al., 2009; Al Shalabi et al., 2012a; Chillingar and Haroun, 2014) in reservoirs.

Electrokinetic (EK) phenomena are among the oldest concepts in surface and colloid science (Wall, 2010). The term “electrokinetics” refers to the motion of small particles in fluids that is induced by an electrical field (Chillingar and Haroun, 2014). The principles of electrokinetic phenomena have been applied in various areas such as soil and groundwater remediation (Wise, 2000; Chillingar and Haroun, 2014), material science (Llorente, et al., 2014), biology and medicine (Abramson, 1934), water treatment (Hayes, 2012; Peraki, et al., 2016), and many others. In particular, EK has been used for decontamination of hydrocarbon polluted soils (Hunter, 1981; Bruell, et al., 1992, Wise, 2000), which involves: (i) electro-migration, (ii) electro-phoresis, and (iii) electro-osmosis processes.

EK has also been proposed for oil recovery in relatively recent years (Amba et al., 1964; Haroun et al., 2009; Wittle and Hill, 2006; Wittle et al., 2011). The electrically enhanced oil recovery method (EEOR) is reported to be capable of increasing oil production with a lower cost and in environments that other enhanced oil recovery (EOR) technologies are unable to produce (Wittle and Hill, 2006; Wittle et al., 2011). The basic premise of the EEOR method is the successful application of the principles of electrokinetics.

As in the case of soil decontamination, when applying electrokinetic principles in EEOR, the main mechanisms involved are hypothesized to be: (i) electro-migration, (ii) electro-phoresis, and (iii) electro-osmosis (Wittle and Hill, 2006; Wittle et al., 2011; Ghazanfari, 2013). Joule heating of the reservoir due to the applied electrical field and electrochemically enhanced reactions are also theorized to contribute to the oil recovery (Wittle and Hill, 2006; Wittle et al., 2011; Ghazanfari, 2013). Electro-osmosis can reduce the amount of water attached to the clay particles, thereby increasing the permeability of the medium and adding a viscous drag of water on the oil phase which results in an increase in the oil production (Cassagrande, 1952; Chillingar et al., 1968). In addition, the electrically induced chemical reactions are hypothesized to cause the so-called “cold cracking” of the complex hydrocarbon compounds into simpler compounds reducing the viscosity of the oil and increasing its mobility (Wittle and Hill, 2006; Ghazanfari, 2013).

The principle idea behind the EEOR method is the application of an electrical field (direct current) directly in the reservoir between a cathode (usually installed in the production well), and anodes (usually installed in injection wells) (Wittle et al., 2011) as

shown in Figure 3.1. Typically, the well configuration is such that a single well is used for injection (anode) and an array of production wells (cathodes) are placed around the injection well (Wittle and Hill, 2006; Wittle et al., 2011).

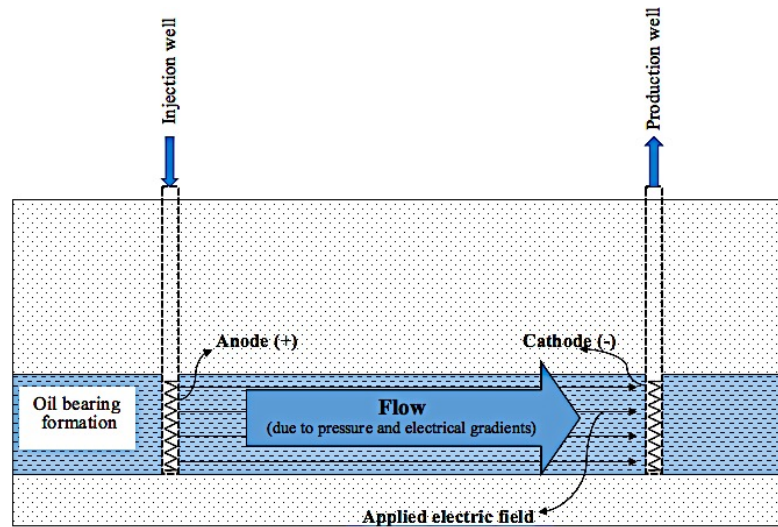


Figure 3.1: Schematic showing field operational of combined water flooding and EEOR

The EEOR method has been tested both at the laboratory scale (Amba et al., 1964; Amba et al., 1965; Haroun et al., 2009; Al Shalabi et al., 2012a) and in the field (United States and Canada) with relatively encouraging results reported (Wittle and Hill, 2006; Wittle et al., 2011). The EEOR method has also been combined with waterflooding in an attempt to increase oil production. It has been reported that this combination has led to an increase in oil recovery by about 10% in laboratory experiments (Al Shalabi et al., 2012b). In the field, EEOR is not usually used as a sole oil recovery method because of the insufficient oil that it produces. However, when combined with waterflooding, it has been found in laboratory experiments (Aggour and Muhammadain, 1992; Al Shalabi et al., 2012b) and in the field (Wittle and Hill, 2006; Wittle et al., 2011) to increase oil recovery.

Although a limited number of laboratory and field investigations have demonstrated the potential promise of the EEOR method, further investigation is necessary to better understand the fundamentals of the method and the importance of different parameters/processes involved in the method. Mathematical models help investigate the feasibility of oil recovery under different reservoir conditions and to provide a fundamental understanding of two-phase flow under reservoir conditions (Amba et al., 1964; Killough and Gonzalez, 1986; Chillingar and Haroun, 2014).

The main objective of this chapter is to use numerical tools to investigate the feasibility of the EEOR method and to provide insight into the important parameters that contribute to the oil production in this method. Specifically, EEOR combined with waterflooding and two-phase flow under coupled pressure and electrical gradients is investigated.

## 3.2 METHODOLOGY

The set of governing equations underpinning the numerical model of the combination of waterflooding with the EEOR method are provided in Section 3.2.1. First, the governing equations for only waterflooding are presented and subsequently the governing equations for the application of the electrical field are introduced. Details of the numerical solution scheme are provided in Section 3.2.2. The steps followed for the numerical simulation are presented in Section 3.2.3. Finally, the description of the set-up of the numerical experiment is provided in Section 3.2.4.

### 3.2.1 GOVERNING EQUATIONS

The first step is the simulation of the effects of waterflooding on pressure and fluid saturations during oil production, without the application of an electrical field involving the EOR method. To simplify the equations involved in the two-phase flow, the following assumptions were made: the two-phases are considered immiscible and incompressible with no exchange of species between them, the rock matrix was assumed to be incompressible, and the total flow rate of oil and water were assumed to remain constant.

#### 3.2.1.1 FLOW DUE TO APPLIED PRESSURE GRADIENT

The governing equation describing two-phase flow due to an applied pressure gradient is the fluid continuity equation (Aziz and Settari, 1979; Chen et al., 2006; Arnes et al., 2007):

$$\frac{\partial(\varphi\rho_{\alpha}S_{\alpha})}{\partial t} + \nabla \cdot (\rho_{\alpha} \cdot \mathbf{v}_{\alpha}) = q_{\alpha} \quad (3.1)$$

where,  $\varphi$  is the porosity of the porous medium,  $\rho_{\alpha}$  is the density of the phase  $\alpha$ ,  $S_{\alpha}$  is the saturation of phase  $\alpha$ ,  $\mathbf{v}_{\alpha}$  is the flow velocity of phase  $\alpha$ , and  $q_{\alpha}$  is the source/sink term. Assuming the density of the phase is constant, we get:

$$\frac{\partial(\varphi S_{\alpha})}{\partial t} + \nabla \cdot \mathbf{v}_{\alpha} = \frac{q_{\alpha}}{\rho_{\alpha}} \quad (3.2)$$

For low flow velocities, Darcy's law is expressed as:

$$\mathbf{v}_{\alpha} = -\lambda_{\alpha} \cdot (\nabla P_{\alpha} + \rho_{\alpha} \mathbf{g} \nabla \cdot \mathbf{z}) \quad (3.3)$$

where,  $\lambda_\alpha$  is the mobility of phase  $\alpha$ ,  $P_\alpha$  is the pressure of phase  $\alpha$ ,  $g$  is the gravitational constant, and  $\mathbf{z}$  is the spatial coordinate in the upward vertical direction.

The phase mobility is defined as (Dake, 1978; Arnes et al., 2007):

$$\lambda_\alpha = \frac{\mathbf{K} k_{r\alpha}}{\mu_\alpha} \quad (3.4)$$

where,  $\mathbf{K}$  is the absolute permeability tensor of the porous medium,  $k_{r\alpha}$  is the relative permeability of phase  $\alpha$ , and  $\mu_\alpha$  is the dynamic viscosity of phase  $\alpha$ . The product of the absolute permeability and the relative permeability of the phase is called the effective permeability of the phase ( $k_\alpha$ ) (Dake, 1978; Bear and Yehuda, 1990).

The relative permeability depends on the saturation of the phase. The set of empirical expressions for the relative permeability of water and oil that are used in this chapter are (Brooks and Corey, 1964):

$$k_{rw} = (S_e)^{\frac{2+3\lambda}{\lambda}} \quad (3.5)$$

$$k_{ro} = (1 - S_e)^2 \left(1 - S_e^{\frac{2+\lambda}{\lambda}}\right) \quad (3.6)$$

where  $\lambda$  is the pore-size distribution index and  $S_e$  is the effective saturation of the water expressed as (Greenkorn, 1983):

$$S_e = \frac{S_w - S_{wc}}{1 - S_{or} - S_{wc}} \quad (3.7)$$

where,  $S_{or}$  is the irreducible oil saturation (i.e. lowest oil saturation that can be achieved)

and  $S_{wc}$  the connate water saturation (i.e. water trapped in the pores of rock during formation of the rock). The viscous coupling effect between phases in the pressure driven flow is considered negligible, and therefore it is not incorporated in the model.

If we substitute Eq. 3.3 into Eq. 3.2 and assume horizontal flow, we get:

$$\frac{\partial(\phi S_{\alpha})}{\partial t} - \nabla \cdot (\lambda_{\alpha} \cdot \nabla P_{\alpha}) = \frac{q_{\alpha}}{\rho_{\alpha}} \quad (3.8)$$

The pressure of the phase can be replaced by a global pressure,  $P$ , if we introduce the fractional flow function,  $f_{\alpha}$ , and assume that at reservoir conditions the viscous forces dominate the effect of the capillary forces (Arnes et al., 2007):

$$P = P_o - P_c \quad (3.9)$$

$$f_{\alpha} = \lambda_{\alpha} \cdot (\lambda_{tot})^{-1} \quad (3.10)$$

$$\lambda_{tot} = \lambda_w + \lambda_o \quad (3.11)$$

where,  $P_o$  is the pressure of the oil phase, and  $P_c$  is a saturation-dependent complementary pressure (Arnes et al., 2007; Ghazanfari, 2013).

$$P_c(S_w) = \int_1^{S_w} f_w(\beta) \frac{\partial P_{cow}}{\partial S_w}(\beta) d(\beta) \quad (3.12)$$

where,

$$P_{cow} = P_o - P_w \quad (3.13)$$

Combing Eqs 3.8 and 3.10, we get:

$$\frac{\partial(\phi S_\alpha)}{\partial t} - \nabla \cdot (\mathbf{f}_\alpha \cdot \nabla P) = \frac{q_\alpha}{\rho_\alpha} \quad (3.14)$$

In most cases, the saturation of water is primarily used, so the equation becomes:

$$\frac{\partial(\phi S_w)}{\partial t} - \nabla \cdot (\mathbf{f}_w \cdot \nabla P) = \frac{q_w}{\rho_w} \quad (3.15)$$

Eq. 3.15 is called the saturation equation. The saturation of oil is calculated using:

$$S_w + S_o = 1 \quad (3.16)$$

The pressure equation is given by the summation of the saturation equations for oil and water combined with Eq. 3.16 as:

$$-\nabla \cdot (\boldsymbol{\lambda}_{\text{tot}} \cdot \nabla P) = \frac{q_w}{\rho_w} + \frac{q_o}{\rho_o} \quad (3.17)$$

To make the pressure equation complete, boundary conditions must be prescribed.

### 3.2.1.2 FLOW DUE TO APPLIED ELECTRICAL GRADIENT

The electro-osmotic (EO) velocity of a phase in a surface-charged porous medium is given by the Helmholtz-Smoluchowski equation as (Smoluchowski, 1914):

$$\mathbf{v}_{e,\alpha} = -\frac{\varepsilon \xi}{\mu} \nabla \Phi_\alpha \quad (3.18)$$

where,  $\varepsilon$  is the permittivity of the medium,  $\xi$  is the zeta potential, and  $\Phi$  is the applied electrical potential.

The electro-osmotic permeability coefficient of the medium is defined as (Ghazanfari, 2013):

$$\mathbf{k}_{eo} = -\frac{\varepsilon\xi}{\mu} \quad (3.19)$$

The electroosmotic flow rate in a porous media is expressed by an empirical equation similar to Darcy's law (Acar et al., 1997):

$$\mathbf{q}_e = -\mathbf{k}_{eo} \cdot \nabla\Phi \quad (3.20)$$

where,  $\mathbf{k}_{eo}$  is the electroosmotic permeability coefficient of the medium.

For two-phase flow (oil and water), the electro-osmotic velocity of a fluid in a surface charged porous medium can be expressed as an extension of the Helmholtz-Smoluchowski equation (see Eq. 3.18) (Ghazanfari, 2013; Chillingar and Haroun, 2014):

$$\begin{bmatrix} \mathbf{v}_{e,w} \\ \mathbf{v}_{e,o} \end{bmatrix} = - \begin{bmatrix} k_{er,ww} & k_{er,wo} \\ k_{er,ow} & k_{er,oo} \end{bmatrix} \mathbf{k}_{eo} \cdot \begin{bmatrix} \nabla\Phi_w \\ \nabla\Phi_o \end{bmatrix} \quad (3.21)$$

where  $k_{er}$  is the relative electro-osmotic permeability.

The viscous coupling between the two phases is considered through the off-diagonal relative electro-osmotic permeability coefficients in Eq. 3.21. In most of the reservoirs, the oil phase is non-polar, hence application of an electrical field does not generate a flow in the oil phase (Ghazanfari, et al., 2014). Therefore,  $k_{er,ow}$  and  $k_{er,oo}$  coefficients are set to zero, and the applied electrical gradient is set to be the same for both phases ( $\Phi$ ) due to the

random distribution of fluids in the reservoir (Ghazanfari, 2013; Chillingar and Haroun, 2014). In this chapter, the coefficients of relative electro-osmotic permeability ( $k_{er,ww}$  and  $k_{er,wo}$ ) are calculated using an empirical correlation developed from available experimental data (Ghazanfari, 2013; Chillingar and Haroun, 2014).

The pressure and saturation equations (Eqs. 3.15 and 3.17) are modified to accommodate the flow generated due to the applied electrical gradient (Eq. 3.21) as:

$$\frac{\partial(\phi S_w)}{\partial t} - \nabla \cdot (\mathbf{f}_w \cdot \nabla P + \mathbf{k}_{eo} k_{er,ww} \cdot \nabla \Phi) = \frac{q_w}{\rho_w} \quad (3.22)$$

$$-\nabla \cdot [\lambda_{tot} \cdot \nabla P + (k_{er,ww} + k_{er,wo}) \mathbf{k}_{eo} \cdot \nabla \Phi] = q \quad (3.23)$$

The first step toward determination of the voltage distribution is the calculation of the total electrical resistivity. Archie's law (Archie, 1942; Bassiouni, 1994; Grattoni and Dawe, 1996; Ferre et al., 1998) is often used in the petroleum industry for this task:

$$R_t = \frac{F R_w}{S_w^n} \quad (3.24)$$

where  $F$  is the formation resistivity factor,  $R_w$  is the electrical resistivity of water,  $S_w$  is the water saturation and  $n$  is a coefficient whose value can be determined from laboratory measurements. The value of the saturation exponent,  $n$ , appears to be close to 2 for sandstone reservoirs (Bassiouni, 1994).

Although, the total resistivity also depends on parameters such as the temperature and the particle size distribution, the effect of saturation dominates over other parameters (Bai et al., 2013). The formation resistivity factor is controlled mainly by porosity and tortuosity,

but tortuosity is almost impossible to measure experimentally. Based on laboratory measurements of  $F$  and  $\phi$  on core samples, the following empirical relationship was suggested (Archie, 1942):

$$F = \phi^{-m} \quad (3.25)$$

An empirical equation, similar to Archie's, that provides a better fit is (**Error! Reference source not found.**, 1952):

$$F = \alpha \phi^{-m} \quad (3.26)$$

where,  $\alpha$  is the coefficient of cementation and  $m$  is the exponent of cementation. Both coefficients are determined experimentally through  $F$ - $\phi$  data.

An extensive collection of  $F$ - $\phi$  data was gathered (1,833 sandstone samples) by Timur et al., 1972 and analysis of the data resulted in the Chevron formula:

$$F = 1.13\phi^{-1.73} \quad (3.27)$$

The equation expressing charge conservation for steady state current is (Avants et al., 1999):

$$\nabla \cdot \mathbf{i} = 0 \quad (3.28)$$

where  $\mathbf{i}$  is the current density.

Per Ohm's law (Avants, et al., 1999; Alshawabkeh, 2001):

$$\nabla \cdot \mathbf{i} = \frac{1}{\rho} \nabla \cdot \mathbf{E} \quad (3.29)$$

where  $\rho$  is the average resistivity of the reservoir and  $\mathbf{E}$  the applied electrical gradient ( $\nabla\Phi$ ). The average resistivity is not the true resistivity, rather it is a weighted average of the resistivity of the reservoir and the various materials that the current encounters (Herman, 2001).

Since an average resistivity is assumed for the reservoir, Eqs. 3.28 and 3.29 lead to Laplace's equation for the applied electrical potential (Avants, et al., 1999; Alshawabkeh, 2001):

$$\nabla \cdot \mathbf{E} = -\nabla^2\Phi = 0 \quad (3.30)$$

To complete Eq. 3.30, boundary conditions must be prescribed.

To summarize, the governing equations used in this chapter are the pressure equation (Eq. 3.23), the saturation equation (Eq. 3.22), and Laplace's equation for the electrostatic potential (Eq. 3.30).

### 3.2.2 NUMERICAL SOLUTION SCHEME

Inspired by the work of Arnes et al., 2007, we used a cell-centered finite volume scheme to solve the governing equations, also referred to as the two-point flux approximation (TPFA) in the literature, and discretized the saturation (Eq. 3.22) and pressure (Eq. 3.23) equations. The scheme uses the cell-averages between each cell and its neighboring cells to approximate the interfacial fluxes due to the applied pressure and electrical potential gradient (Arnes et. al., 2007).

The Implicit-Pressure-Explicit-Saturation (IMPES) method was used to solve the pressure (Eq. 3.23) and saturation equations (Eq. 3.22). IMPES is a scheme employed for problems with intermediate difficulty and nonlinearity (e.g. two-phase incompressible flow) and is popular in the petroleum industry (Chen et al., 2006). The main advantage of the scheme is the separation of the computation of pressure from the computation of saturation by obtaining a single pressure equation from the combination of the flow equations (Aziz and Settari, 1979; Chen, et al., 2004). The pressure is advanced implicitly in time and the saturation is updated explicitly. Despite the advantages of the method, it also involves stability issues that originate from the explicit solution of the saturation equation (Aziz and Settari, 1979). To overcome this issue, small time steps can be used, however this leads to additional computational effort and may render the method inapplicable for extremely computationally-challenging problems (Chen et al., 2004).

Because we solve the saturation explicitly, we need to ensure that we impose a stability condition, which is called the Courant-Friedrichs-Lewy (CFL) condition, on the time step. For that reason, the solution of the saturation equation included local time steps that ensured the stability at each global time step. Adhering to this condition ensured that the water saturation did not take values less than  $S_{wc}$  or greater than  $(1-S_{or})$ . The imposed condition in this case was (Arnes et al., 2007):

$$\Delta t \leq \frac{\varphi |\Omega_i|}{u^{in} \max\{f'(s)\}_{0.2 \leq s \leq 0.8}} \quad (3.31)$$

$$u^{\text{in}} = \max(q, 0) - \sum_j \min(u)_{\text{pressure}} - \sum_j \min(u)_{\text{voltage}} \quad (3.32)$$

$$f'(s) = \frac{1}{1 - S_{\text{wc}} - S_{\text{or}}} \frac{\partial f}{\partial S_e} \quad (3.33)$$

where  $\Delta t$  is the local time step,  $|\Omega_i|$  is the area of the finite volume cell,  $u^{\text{in}}$  is the inflow flux of the cell,  $(u)_{\text{pressure}}$  is the cell interface fluxes due to the pressure gradient,  $(u)_{\text{voltage}}$  is the interface flux due to voltage gradient, and  $f$  is the fractional flow.

The local time step condition depended on the saturation only through the flux, so the new local time step was modified every time a new solution to the pressure equation was computed.

The heterogeneity of reservoirs causes issues of up-scaling when moving from the core scale to the reservoir scale. In particular, the values of absolute hydraulic permeability, porosity, relative hydraulic permeability, and absolute and relative electroosmotic permeability are usually determined at the core scale, which causes problems when using these values at the reservoir scale (Ghazanfari, 2013). In this chapter, we are considering a homogeneous and isotropic reservoir to limit the effects of upscaling without, however, eliminating it completely.

### 3.2.3 SIMULATION STEPS

The steps followed for the numerical simulation were:

- a. Input of primary parameters (e.g. geometry of reservoir, geometry of cells, properties of medium, properties of fluids, injection rate, applied current density, resistivity of water, time parameters).
- b. Input of initial saturation and calculation of initial saturation-dependent electrical properties (e.g. resistivity, voltage gradient, relative electroosmotic permeability).
- c. Calculation of initial saturation-dependent coefficients (pressure and voltage) for the pressure equation.
- d. Calculation of voltage and pressure distributions (implicitly).
- e. Calculation of flux caused by pressure and voltage gradients.
- f. Calculation of local time step for stability.
- g. Calculation of water saturation of the next time step (explicitly).
- h. Calculation of saturation-dependent electrical properties of the next time step.
- i. Calculation of saturation-dependent coefficients (pressure and voltage) for the next time step.
- j. Repeat steps d to i until the end of the simulation period.

### 3.2.4 NUMERICAL-EXPERIMENT SET-UP

As mentioned in Section 3.2.1, the well configuration in the EEOR method is typically such that a single well is used for injection (anode) at the center of the reservoir and an array of four production wells (cathodes) are placed around the injection well on the four corners of the reservoir (Wittle and Hill, 2006; Wittle, et al., 2011). To facilitate the initial implementation of the equations and for simplicity, a system of one injection well and one production well placed in opposite corners of a hypothetical 2-D sandstone reservoir was used. The grid consisted of square cells with dimensions of  $120 \times 220 \times 1$  grid-blocks, with 26,400 cells in total. The selected parameters for the reservoir were taken from reasonable ranges available in the literature (Brooks and Corey, 1964; Okandan, 1984; Bassiouni, 1994; Alshawabkeh, 2001; Christle and Blunt, 2001; Sadikh-Zadeh, 2006; Wittle and Hill, 2006; **Error! Reference source not found.**, et al., 2007; Wittle, et al., 2011; Ghazanfari, et al., 2014; Chilingar and Haroun, 2014) and are presented in Table 3.1.

For the pressure equation (Eq. 3.23), no-flow boundary conditions around the reservoir were imposed (Aziz and Settari, 1979; Chen, et al., 2006; Arnes, et al., 2007). Typically for field applications of the EEOR method, the current density is maintained constant and no flow of electrical current is assumed through the boundaries of the examined reservoir (Avants, et al., 1999; Alshawabkeh, 2001). Similar to the pressure equation, values were assigned to the electrodes to facilitate the calculation of electrical potential using Eq. 3.30(Avants, et al., 1999; Alshawabkeh, 2001):

$$\Phi|_{\text{anode}} = \Phi_{\text{max}} \quad (3.34)$$

$$\Phi|_{\text{cathode}} = 0 \quad (3.35)$$

where,  $\Phi_{\text{max}}$  is the maximum applied voltage calculated by:

$$\Phi_{\text{max}} = E_{\text{electrodes}}R \quad (3.36)$$

where,  $E_{\text{electrodes}}$  is the applied voltage gradient between the electrodes, and  $R$  is the distance between the anode and cathode (diagonal of reservoir). The  $E_{\text{electrodes}}$  is calculated every time the saturation changes using Eq. 3.29.

Table 3.1: Characteristics of reservoir used in numerical simulation

Parameter	Value
Dimensions of reservoir	120 m × 220 m
Porosity	0.2
Absolute permeability	100 mD
Absolute electro-osmotic permeability	$1 \cdot 10^{-9} \text{ m}^2/(\text{Volt} \cdot \text{sec})$
Viscosity of water	$3 \cdot 10^{-4} \text{ kg}/(\text{m} \cdot \text{s})$
Viscosity of crude oil	$3 \cdot 10^{-3} \text{ kg}/(\text{m} \cdot \text{s})$
Irreducible oil saturation	0.2
Connate water saturation	0.2
Initial water saturation	0.4
Initial oil saturation	0.6
Injection rate	9.15 m <sup>3</sup> /day
Pressure at production well	$\sim 3 \cdot 10^7 \text{ Pa}$
Salinity of water phase	0.5 Ω.m
Applied current density	1 A/m <sup>2</sup>

The coefficient matrix of the pressure equation that includes the total mobility of the phases (Eqs. 3.11 and 3.23) demonstrates an inherent singularity in the problem that is

usually overcome by setting a constant value of pressure thereby ensuring a unique solution (Arnes, et al., 2007). In this chapter, the global pressure at the production well was set to a fixed value (Table 3.1) based on available reasonable values from the literature (Christle and Blunt, 2001). The total simulation period was set to 1,000 days with a global time step of 1 day. Each global time step was solved as many times (local time steps) as required to maintain the stability of the solution (Eq. 3.31).

Figure 3.2 and Figure 3.3 present the pressure and the voltage distribution, respectively, at various times. The pressure and the voltage appear to follow the same distribution pattern with the highest values being at the injection well, as expected. The maximum value of both pressure and voltage parameters at the injection well decreases as the waterfront propagates toward the production well, while the values further away from the injection well start to increase until they reach the proximity of the production well. As the water saturation in the reservoir increases, the resistivity of the medium decreases, and consequently, for a constant applied current density, the voltage drops (see Eq. 3.29).

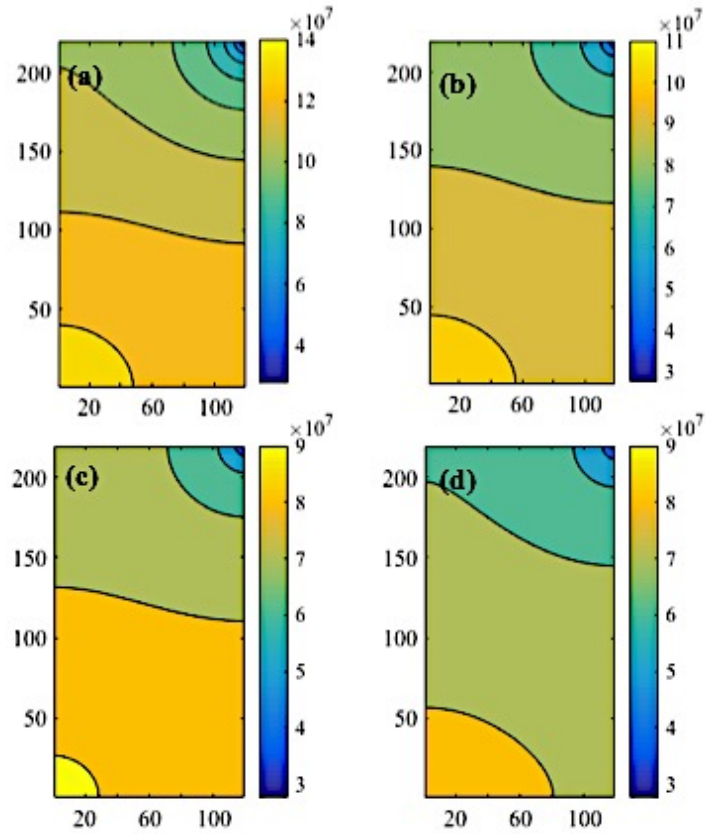


Figure 3.2: Pressure distribution (in Pa) in the reservoir at: (a) 250 days, (b) 500 days, (c) 750 days, and (d) 1,000 days. The injection well is located at the lower left corner and the production well is located at the upper right corner

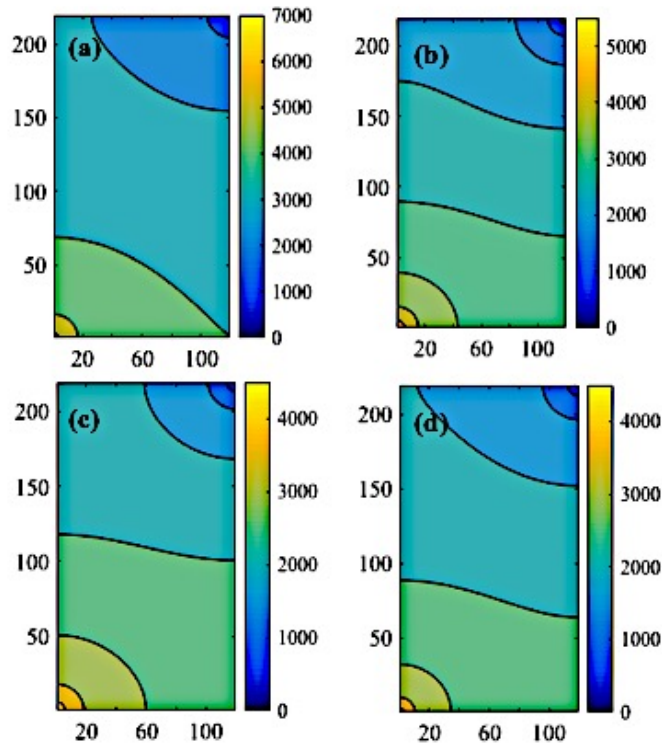


Figure 3.3: Voltage distribution (in Volt) in the reservoir at: (a) 250 days, (b) 500 days, (c) 750 days, and (d) 1,000 days. The injection well is located at the lower left corner and the production well is located at the upper right corner

The water front appears to reach the production well at around 100 days, as can be seen in Figure 3.4. It appears to move faster at the middle of the reservoir until it reaches the production well (Figure 3.4 (b) and (c)), and then it expands toward the boundaries of the reservoir (Figure 3.4 (d)).

Since adequate EEOR field data were not available in the literature to allow the calibration of the developed model, an analysis was performed to examine the model sensitivity to various parameters related to the reservoir. In order to compare the results from the analysis, the cumulative oil production (i.e. the gross amount of oil produced over a time period) was calculated under different scenarios and the results are presented in the

following section. Then, the effects of important operational parameters on oil production were investigated to gain an insight into the importance of different parameters involved in the combined water flooding and EOR method.

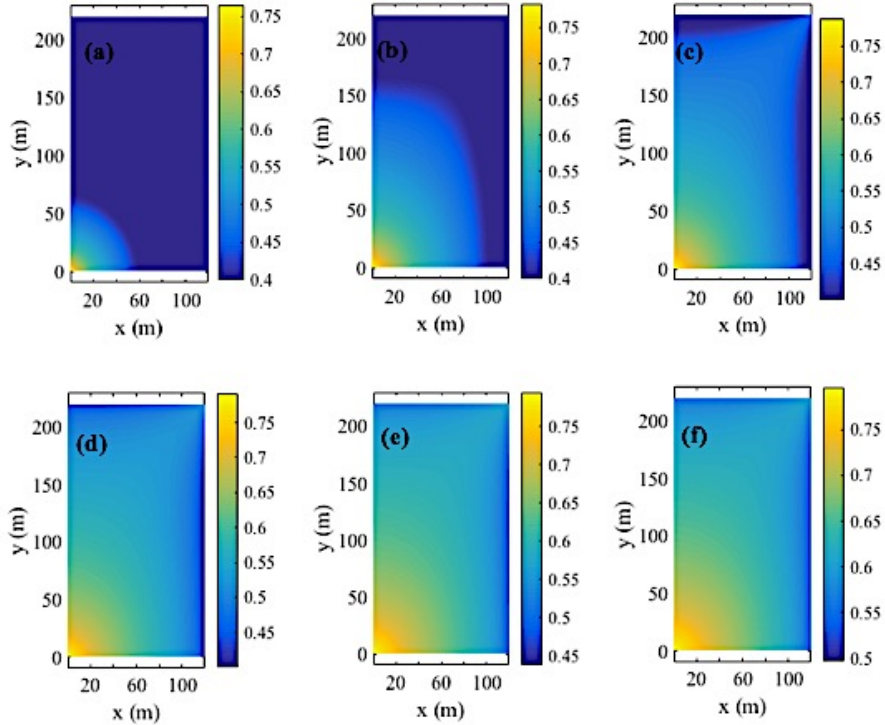


Figure 3.4: Water saturation distribution at: (a) 10 days, (b) 50 days, (c) 100 days, (d) 200 days, (e) 500 days, and (f) 1,000 days. The injection well is located at the lower left corner and the production well is located at the upper right corner

### 3.3 RESULTS AND DISCUSSION

The results of the sensitivity analysis performed on the parameters related to the reservoir are presented in Section 3.3.1. The effects of important operational parameters on oil production are demonstrated in Section 3.3.2 and, finally, a comparison of the two-phase flow in the water flooding method with that of the combined water flooding and

EEOR method is provided in Section 3.3.3.

### 3.3.1 SENSITIVITY ANALYSIS

The sensitivity analysis was performed on important reservoir parameters involved in the combined water flooding and EEOR method. The reservoir parameters included porosity, absolute electro-osmotic permeability, relative hydraulic and electro-osmotic permeability, initial water saturation, and oil viscosity.

#### 3.3.1.1 POROSITY

The porosity ( $\phi$ ) of the reservoir is usually closely related to the permeability such that different empirical correlations and models have been developed to predict the permeability of the reservoir using porosity measurements (Handhal, 2016). Similar to the permeability, reservoirs usually have heterogeneous porosity distributions (Islam, et al., 2010), however, for the purpose of this analysis, the reservoir is considered to be homogeneous with constant porosity. The range of porosity values selected for sandstone in this analysis is 0.1 to 0.3 (Sadikh-Zadeh, 2006). As shown in Figure 3.5(a), the porosity value significantly affected the cumulative oil production. For instance, a 50% decrease of porosity resulted in about a 37% decrease in cumulative oil production at 1,000 days. This was expected as the change in the reservoir porosity results in a change in the available pore space, and thus, the change in the amount of oil stored in the reservoir.

In addition, the porosity affected the flow due to the applied electrical field. Eqs. 3.24 and 3.27 indicate that an increase in the porosity of the reservoir will result in a decrease in the total resistivity. Since in the EEOR method the applied current density is

usually kept constant, the reduction in the total resistivity will, in turn, result in an increase of the voltage gradient and subsequently, an increase in the flow (i.e. oil production) (Eq. 3.29).

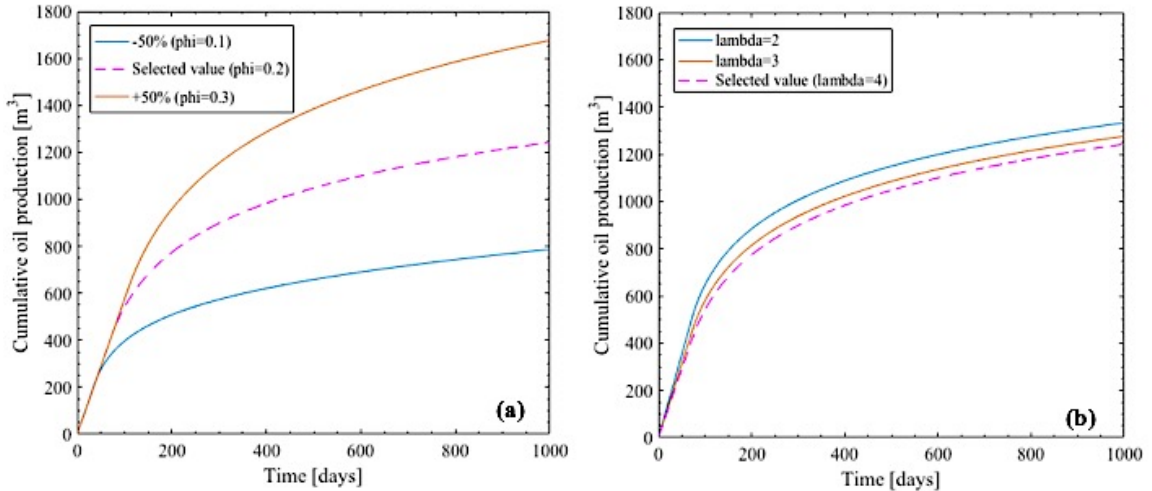


Figure 3.5: Variation of cumulative oil production with (a) porosity ( $\phi$ ) and (b) with relative hydraulic permeability ( $k_{r,w}$  &  $k_{r,o}$ ) coefficients. Different values of pore size distribution index ( $\lambda$ ) were used for the estimation of the relative hydraulic permeability coefficients

### 3.3.1.2 RELATIVE HYDRAULIC PERMEABILITY COEFFICIENTS

The relative hydraulic permeability of both phases mainly depends on the water saturation (see Eqs. 3.5 and 3.6). Another parameter involved in the estimation of the relative permeability coefficients is the pore size distribution index,  $\lambda$  (Brooks and Corey, 1964; Li, 2004), which is determined experimentally. A typical range of  $\lambda$  values for sandstones is between 2 and 4 (Brooks and Corey, 1964). Hence, the selected  $\lambda$  values for the sensitivity analysis were 2, 3, and 4.

The results of the sensitivity analysis are presented in Figure 3.5(b). As the value of the pore distribution index increased, the cumulative production of oil decreased. This can be explained by examining Eqs. 3.5 and 3.6. When the value of  $\lambda$  increases, the equations will calculate a higher value of relative permeability of water and a lower relative permeability of oil compared to cases for lower values of  $\lambda$ . Therefore, the mobility of water increases and the mobility of oil decreases, which in turn results in the oil production drop.

### 3.3.1.3 ABSOLUTE ELECTRO-OSMOTIC PERMEABILITY

While the absolute permeability is influenced by the pore size and pore distribution in the medium, the absolute electro-osmotic permeability is mainly dependent on the porosity (Alshawabkeh, 2001). The absolute electro-osmotic permeability of soils and rocks is reported to be in the order of  $10^{-9} \text{ m}^2/(\text{Volt}\cdot\text{s})$  (Alshawabkeh, 2001). For this sensitivity analysis, the value of  $k_{eo}$  was altered lower and higher by an order of magnitude than the selected value of  $10^{-9} \text{ m}^2/(\text{Volt}\cdot\text{s})$  and the results are shown in Figure 3.6. Lowering  $k_{eo}$  by one order of magnitude had negligible effect on the oil production. This might be attributed to the fact that the selected electro-osmotic permeability value of  $10^{-9} \text{ m}^2/(\text{Volt}\cdot\text{s})$  is a low value, and therefore, the application of the electrical field did not result in significant flow and the total cumulative production almost matched the production due to only water flooding. However, increasing the  $k_{eo}$  value to  $10^{-8} \text{ m}^2/(\text{Volt}\cdot\text{s})$  resulted in about a 20% increase in the cumulative oil production, thus rendering  $k_{eo}$  an important parameter for the application of the method. The increase in the cumulative oil production was mostly due to the flow induced by the applied electrical field as the absolute electro-osmotic

permeability only appears in the electrical part of the governing equations for the two-phase flow.

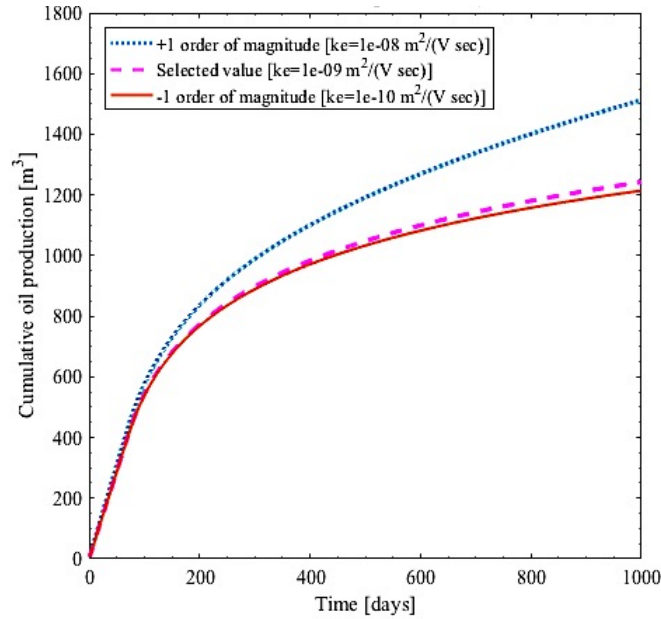


Figure 3.6: Variation of cumulative oil production with absolute electroosmotic permeability ( $k_{eo}$ )

### 3.3.1.4 RELATIVE ELECTROOSMOTIC PERMEABILITY COEFFICIENTS

The relative electro-osmotic permeability coefficients (Eq. 3.21) for water ( $k_{er,ww}$ ) and water-oil phase ( $k_{er,wo}$ ) are saturation-dependent parameters. The  $k_{er,ww}$  is the relative electro-osmotic permeability of only the water phase while  $k_{er,wo}$  captures the “drag” of the water on the oil phase due to the applied electrical field (Ghazanfari, et al, 2014). In this chapter, the available empirical correlations developed for these coefficients in sandstone reservoirs (Ghazanfari, et al., 2014; Chillingar and Haroun, 2014) were used. Compared to the coefficients for relative hydraulic permeability, these coefficients are much smaller, particularly  $k_{er,wo}$  (Ghazanfari, et al., 2014; Chillingar and Haroun, 2014).

To account for variability, the sensitivity analysis scenarios were performed by altering the values of  $k_{er,ww}$  and  $k_{er,wo}$  by 20% and 50% for each time step involved in the simulation.

Figure 3.7(a) and 3.7(b) present the results of sensitivity analysis for  $k_{er,ww}$  and  $k_{er,wo}$ , respectively. The change in neither coefficient seems to significantly affect the cumulative oil production. The minor importance of these coefficients can be attributed to the fact that these coefficients were multiplied by the absolute electro-osmotic permeability parameter, which was on the order of  $10^{-9} \text{ m}^2/(\text{Volt}\cdot\text{s})$ . Hence, these changes did not significantly affect the flow outcome (Eqs. 3.22 and 3.23). It is also important to note that  $k_{er,wo}$ , in particular, was less than 0.1 for a wide range of water saturations (Ghazanfari, et al., 2014; Chillingar and Haroun, 2014), which might explain the fact that a change in its magnitude had an insignificant effect on flow.

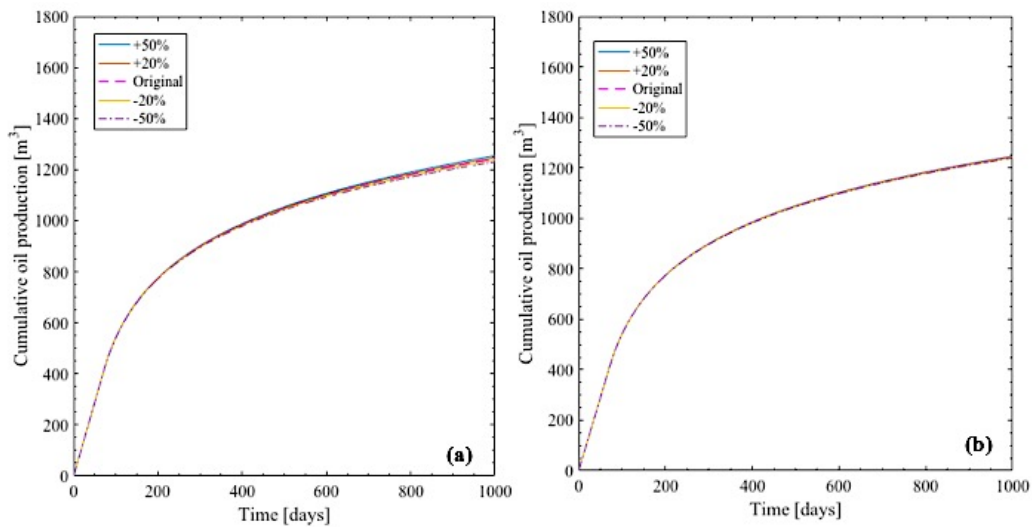


Figure 3.7: Variation of cumulative oil production with (a) relative electroosmotic permeability of water ( $k_{er,ww}$ ) coefficient and (b) relative electroosmotic permeability of water-oil ( $k_{er,wo}$ ) coefficient

### 3.3.1.5 INITIAL WATER SATURATION

The initial water saturation is an important parameter for the evaluation of an oil reservoir and one of the most challenging parameters to quantify (Ringen, et. al, 2001). The importance of the parameter is due, as seen in the governing equations presented in Section 3.2.1, to the many saturation-dependent parameters that control the flow. The water saturation not only influences the flow due to the pressure gradient but also plays a major role in the parameters controlling the flow due to the applied electrical gradient (e.g. reservoir resistivity). In addition, water saturation controls the volume of oil that is stored/available in the reservoir. Figure 3.8(a) presents the results for the cumulative oil production for different initial water saturations. As expected, the higher water saturations produced less oil (i.e. 80% lower for a 50% increase in the water saturation) than the lower ones (up to 45% more oil for a 25% decrease in initial water saturation).

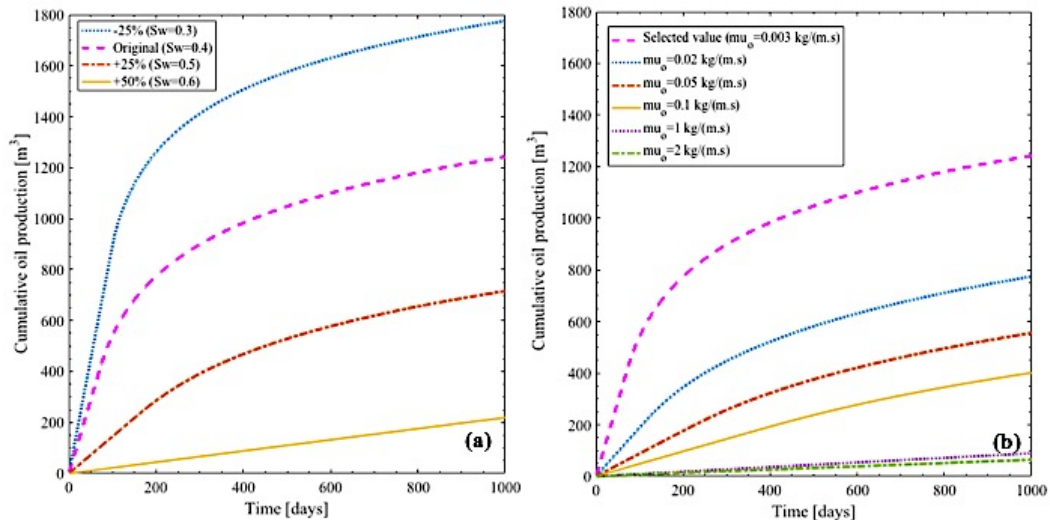


Figure 3.8: Variation of cumulative oil production with (a) initial water saturation ( $S_w$ ) and (b) oil viscosity ( $\mu_o$ )

### 3.3.1.6 OIL VISCOSITY

One of the main characteristics of crude oil, that renders its extraction challenging, is its low mobility (Okandan, 1984). The mobility of a phase (see Eq. 3.4) depends on: (i) the absolute permeability of the porous media, (ii) the relative hydraulic permeability of the phase (saturation-dependent), and (iii) the viscosity of the phase. The effects of the first two parameters on the flow were investigated in previous sections. The viscosity of crude oil usually ranges from 0.003 to 10 kg/(m·s) (Okandan, 1984; Ghazanfari, et al., 2014; Guo, et al., 2016). In this chapter, we used a light crude oil with a viscosity of  $\mu_o=0.003$  kg/(m·s).

To examine the effect of the oil viscosity on the flow, a wide range of viscosity values (0.003 to 2 kg/(m·s)) were selected for the sensitivity analysis. As expected, the results of the analysis show that higher oil viscosity resulted in less oil production, as shown in Figure 3.8(b). For example, the reservoir with lighter oil in Figure 3.8(b) produced 98% more oil than the heaviest oil case. This significant difference in oil production indicated that a reservoir with such high-viscous oil might not be exploitable by the combination of water flooding and EOR methods.

For simplicity, the reservoir was considered to be homogeneous and isotropic, hence, the value of the absolute permeability remained constant within the reservoir. Due to the assumption of a steady-state homogeneous medium, the absolute hydraulic permeability did not affect the flow and was not included in the sensitivity analysis. This may be explained by examining Eqs. 3.4, 3.8, and 3.22. The absolute permeability does not contribute to the saturation equation (Eq. 3.22), because it gets cancelled in Eq. 3.8 where

the fractional flow of each phase was calculated as a ratio of the phase mobility of the phase and the total mobility.

### 3.3.2 EFFECTS OF OPERATIONAL PARAMETERS ON FLOW

The sensitivity analysis provided in the previous section showed that the developed model was capable of responding properly to changes in the important reservoir parameters affecting oil production. To gain a better understanding of the contribution of an applied electrical field to the flow in the EOR method, the effects of important operational parameters on oil production were investigated.

#### 3.3.2.1 APPLIED CURRENT DENSITY

One of the most important parameters to consider for the application of an electrical field to an oil reservoir is the applied current density. The current density not only affects the amount of extracted oil due to the applied electrical gradient (Eq. 3.29), but also primarily controls the cost of the EOR method (Wittle and Hill, 2006; Wittle, et al., 2011). Usually, in the field, the current density is maintained constant. The lowest feasible applied current density is  $0.1 \text{ A/m}^2$  and the highest is no more than  $5 \text{ A/m}^2$  (Wittle and Hill, 2006; Wittle, et al., 2011; Chillingar and Haroun, 2014). In this chapter, the selected value was  $1 \text{ A/m}^2$  and the range of current density for the sensitivity analysis was  $0.1$  to  $5 \text{ A/m}^2$ . As can be seen in Figure 3.9(a), a decrease in applied current density of 90% resulted in about 4% less oil production. To achieve a 4% and 8% increase in the oil production, the current density was increased by 100% and 400%, respectively. As expected, the current density

was found to be an important parameter in the EOR method as it affected the flow due to the applied electrical field.

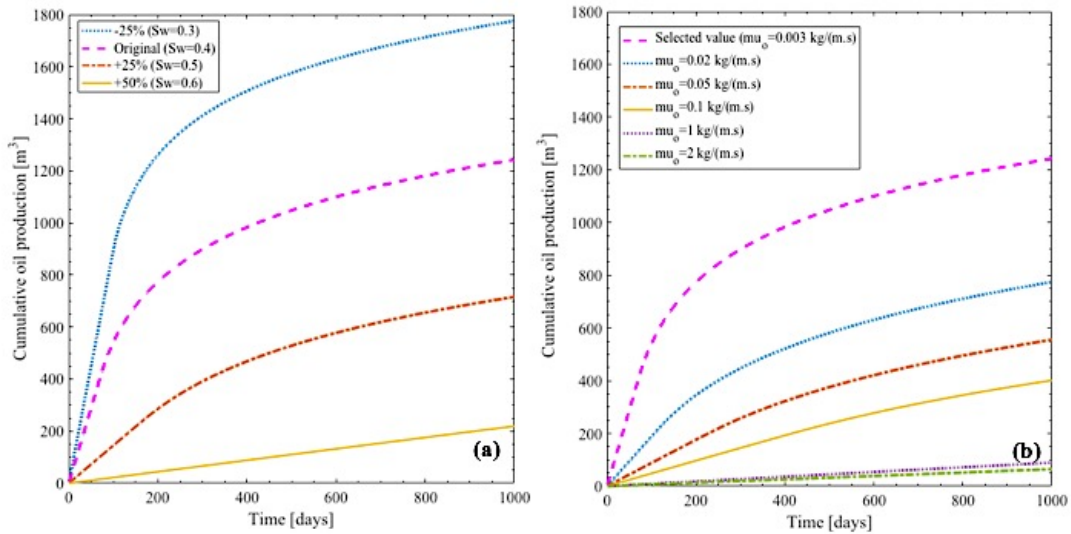


Figure 3.9: Variation of cumulative oil production with (a) applied current density ( $i$ ) and (b) water resistivity ( $R_w$ )

### 3.3.2.2 RESERVOIR RESISTIVITY

Reservoir resistivity affects current flow, and in turn oil production (Eq. 3.24) due to an applied electrical field. The applied electrical gradient is proportional to the average resistivity of the reservoir (Eq. 3.29). Therefore, a decrease in the resistivity, while maintaining a constant current density, will result in a decrease of the applied voltage gradient, and thus in a decrease in the fluid flow due to applied electrical field (Eq. 3.20). The resistivity of the water (and in turn the reservoir) varies with the salinity of the injected water (Bassiouni, 1994).

A wide range of water resistivity values was selected to represent the variability in the salinity of the injected water. The higher values of resistivity were selected because of the low-salinity water-flooding techniques that are implemented in some cases (Sheng, 2014). Figure 3.9(b) demonstrates the results of the simulations for various water resistivity values. The higher resistivities appear to produce more oil than the those with the lower resistivities thereby validating the relationship between voltage gradient and resistivity.

The water resistivity appears only in the equations for the electrical part of the flow, meaning that the increase in oil recovery is mainly driven by the applied electrical field. The developed model assumed immiscible flow, and therefore, the effects of changes in the salinity of water on the pressure-driven flow were not considered.

### 3.3.2.3 INJECTION RATE

It is intuitive that higher water injection rates will lead to higher oil production due to an increase in the pressure difference between the injection and the production wells. Figure 3.10 shows a 20% increase in oil production for a 200% increase in the water injection rate. However, it should be noted that this high injection rate might not be practical in the field. Also, it should be noted that the increase in the water injection rate might adversely affect the electrical part of the flow (lower resistivity results in lower voltage gradient, see Section 3.3.2.2), but this effect is shadowed by the greater effect of the pressure driven part of the oil production.

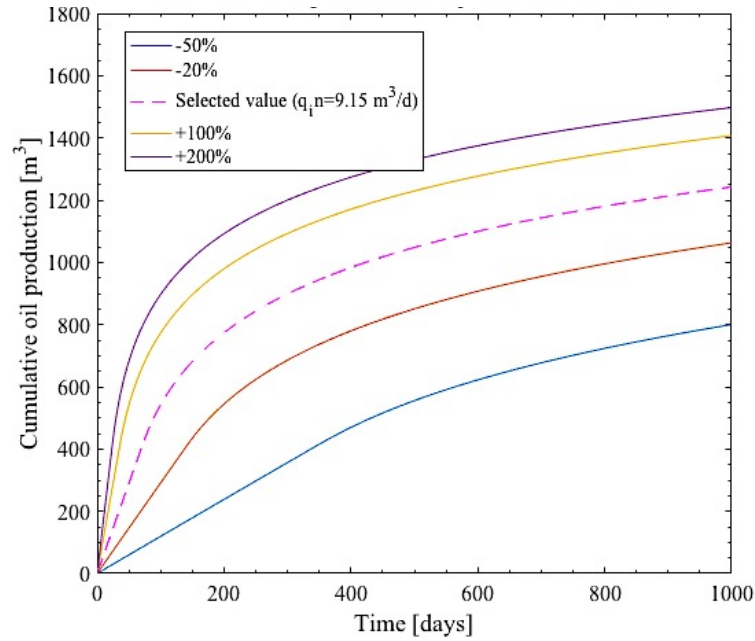


Figure 3.10: Variation of cumulative oil production with applied water injection rate ( $q_{in}$ )

### 3.3.3 COMPARING FLOW IN WATERFLOODING WITH THAT OF COMBINED WATERFLOODING AND EEOR

In order to investigate the feasibility of implementing the EEOR method for oil production, a comparison of oil production between water flooding alone and water flooding combined with EEOR was performed. All the parameters for the two cases (i.e. only water flooding, and water flooding with EEOR) were identical except for the electrical parameters that were only present in the combination of water flooding with EEOR.

Figure 3.11 demonstrates the results of this comparison. The combination of the two methods appears to result in an additional 4% cumulative oil production after 1,000 days. This 4% increase is attributed to the application of EEOR and is consistent with the reported values in the literature (Wittle and Hill, 2006; Wittle, et al., 2011; Al Shalabi, et

al., 2012b). If the result from the water flooding alone case is compared to the result from the 5 A/m<sup>2</sup> applied current density (see Figure 3.9(a) and Figure 3.11), the oil production was 12% higher for the combination of the two methods. However, the application of EEOR is much more costly for a current density of 5 A/m<sup>2</sup> compared to the selected current density of 1 A/m<sup>2</sup> (Chillingar and Haroun, 2014).

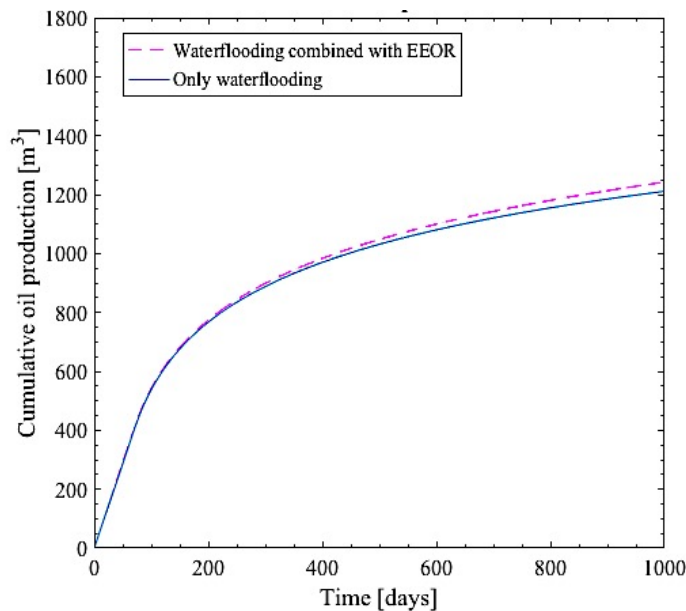


Figure 3.11: Comparison of cumulative oil production for two cases: (i) only waterflooding, and (ii) combination of waterflooding and EEOR method

### 3.4 SUMMARY

This chapter numerically investigated the two-phase immiscible fluid flow involved in the application of the EEOR method to an oil reservoir. A numerical experiment was designed to evaluate the importance of different parameters involved in EEOR combined with water flooding. A sensitivity analysis was performed to examine the sensitivity of the developed model to various reservoir parameters and then to evaluate the

importance of field operational parameters. In addition, the contribution of the applied electrical field to the flow was investigated.

The sensitivity analysis showed that porosity, absolute electro-osmotic permeability, initial water saturation, oil viscosity, applied current density, water resistivity, and water injection rate are important parameters affecting oil production using this method.

In addition, the results presented in this chapter showed that the applied electrical gradient involved in EEOR combined with the water flooding method contributed to a very small increase in oil production. It should be noted that the reported conclusions were based on many assumptions and the authors acknowledge the limitations involved in the development and application of this numerical simulation due to scarcity of adequate experimental and field data on the EEOR method for calibration of the model. Future work may include improvements in the model such as (i) evaluation of the effects of different well configurations (anode, cathode configurations) on oil production, (ii) incorporating the effects of the applied electrical field on the oil viscosity and coefficients of relative hydraulic permeability, (iii) fully coupling the pressure and electrical gradients, and (iv) incorporating the non-isothermal effects due to joule heating of the reservoir.

## CHAPTER 4

# INVESTIGATION OF THE FEASIBILITY OF CRUDE OIL VISCOSITY CHANGE UNDER APPLIED ELECTRICAL FIELD IN POROUS MEDIA AND ITS SIGNIFICANCE FOR TRANSPORT PHENOMENA

### ABSTRACT

The electrically enhanced oil recovery (EOR) method takes advantage of electrokinetic phenomena. One of the hypothesized underlying mechanisms involved in this method is the reduction of crude oil viscosity due to an applied electrical field, and therefore an increase in the oil mobility. This chapter investigates the feasibility of oil viscosity change due to an applied electrical field and its importance in transport phenomena during oil recovery using experimental and numerical tools. The physical experiment simulated the application of an applied electrical field to a synthetic formation in a small-scale test cell. The results of the physical experiment indicated a slight reduction in the oil viscosity at the center region of the test cell. To examine the effect of the change in oil viscosity on transport, a numerical experiment was performed. The data from this experiment and from other experimental and field applications available in the literature were used to linearly interpolate the value of the oil viscosity with time. The results of the numerical experiments indicated that incorporating the changes in the oil viscosity leads to a considerable increase in the cumulative oil production, whose magnitude depends on the magnitude of viscosity change due to the electrical field application.

## 4.1 INTRODUCTION

Applications of flow and transport phenomena in porous media are encountered in soil science, groundwater hydrology, petroleum industry, storage of energy byproducts in deep geological formations (e.g. carbon storage, nuclear waste disposal), and biomedical engineering among others (Greenkorn, 1983; Weir, et al., 1996; Khaled and Vafai, 2003; Bauer et al., 2008; Ju, 2014; Kim, et al., 2014; Shi et al., 2016). The study of flow and transport phenomena in porous media is complex due to several factors including the interactions between multiple fluid phases, fluid phases and pore structure, and associated physio-chemical processes (Al-Khlaifat and Arastoopour, 2001; Pinder and Gray, 2008; Rajagopal and Srinivasan, 2014).

The electrokinetic phenomena are a driving force for mass transport in porous media in several applications. Electrokinetics refers to the movement of small particles in fluids due to an applied electrical field (Acar and Alshwabkeh, 1993; Pamukcu et al., 2009; Electorowicz, 2009; Pamukcu and Ghazanfari, 2014). Electrokinetic technology has been traditionally implemented in environmental applications for the decontamination of polluted sites (Alshwabkeh et al., 1996; Pamukcu et al., 2009). The method relies on applying a low direct current (DC) electrical field to activate electro-kinetic (EK) phenomena in the porous media to transport the water, solutes, and charged colloids present in the pore space toward one of the electrodes (Pamukcu et al., 2009).

The application of electrokinetics for mass transport in porous media has been extended to other areas such as environmental mitigation of hydrocarbon-contaminated sites (e.g. Bruell et al., 1992; Pamukcu et al., 1995; Saichek and Reddy, 2005; Korolev et

al., 2008), and for recovery of reservoir oil (e.g. Amba et al., 1965; Wittle et al., 2008; Alshalabi et al., 2012; Ghazanfari and Pamukcu, 2014). The basic premise of electrically enhanced oil recovery (EEOR) method is successful application of the principles of electrokinetics. The method utilizes an applied direct current (DC) electrical field in the reservoir between a cathode and anode installed in the injection and production wells (Wittle et al., 2008; Alshalabi et al., 2012; Hill, 2014) as shown in Figure 4.1. The typical well configuration involves a single well for injection (anode) and an array of production wells (cathodes) placed around the injection well (Wittle et al., 2008; Alshalabi et al., 2012; Hill, 2014). In the field, EEOR is not usually used as a sole enhanced oil recovery method because of the insufficient oil that it produces. In order to improve the efficiency, the method is usually combined with water flooding (Wittle et al., 2008; Alshalabi et al., 2012; Hill, 2014), where water is injected into the reservoir and the water front displaces the oil toward the production wells (Latil, 1980).

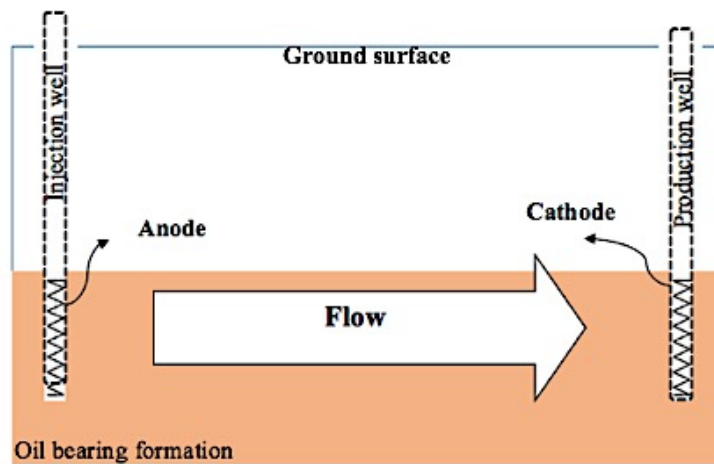


Figure 4.1: Schematic showing the field operation of EEOR method

Some of the mechanisms involved in EEOR are hypothesized to be: (i) electro-migration, (ii) electro-phoresis, (iii) electro-osmosis, and (iv) electrochemically enhanced reactions (Wittle et al., 2008; Alshalabi et al., 2012; Hill, 2014). Electro-migration is the movement of dissolved ionic components under the influence of an electrical field (Pamukcu, 2009). The migration of the charged colloids toward the anode (e.g. clay particles) is called electro-phoresis and is reported to potentially unclog some of the pore-throats, thereby improving the permeability of porous media (e.g. Chilingar et al., 1968; Ghazanfari, 2013; Ghazanfari and Pamukcu 2014). Electrophoretic transport may contribute to oil production when the hydrophobic molecules are adsorbed to the surface charged colloidal particles (Wittle et al., 2008; Hill et al., 2014). The movement of ionic fluids within clay's double layer is called electro-osmosis. It is hypothesized that electroosmotic flow will be activated near the solid-liquid interface due to applied DC electrical field. This leads to increased oil recovery due to viscous drag of the water phase on the non-polar oil phase (e.g. Wittle et al., 2008; Hill, 2014; Ghazanfari et al., 2014). In addition, the applied electrical field changes the chemistry of the pore fluid and the soil/rock formation. The resulting electrically induced chemical reactions are postulated to cause transformation of the oil, resulting in reduction of the oil viscosity (Wittle et al., 2008; Ghazanfari, 2013; Hill, 2014). This transformation is suggested to occur when the complex hydrocarbon compounds break into simpler compounds, a phenomenon called "cold cracking", that reduces the viscosity of the oil and increases its mobility (Wittle et al., 2008; Ghazanfari and Pamukcu 2014; Hill, 2014).

The "cold cracking" phenomenon has been mostly studied as it relates to the oil refinement process (NETL report, 2006). Radiation, microwaves, and electromagnetic

pulses are among the methods that have been used to trigger the change in the oil composition (e.g. Tao and Xu, 2006; Bientinesi et al., 2013). The contribution of oil viscosity change to the flow in the EOR method has been studied to some extent (Wittle et al., 2008; Ghazanfari, 2013). Wittle et al., (2008) conducted large-scale laboratory experiments on a synthetic formation, simulating the EOR process, and reported a change in the Gas Chromatography Mass Spectrograph (GCMS) spectra of the crude oil due to application of a low DC electrical field. They compared the GCMS spectra of the crude oil at the beginning of the experiment and after 27 days of applying a low DC electrical field to the synthetic formation, and reported that the molecular abundances in the more complex hydrocarbons reduced while the molecule abundances of the simpler components increased. Ghazanfari (2013) reported a change in the crude oil viscosity in laboratory experiments simulating EOR for different crude oils. The reported SARA (Saturates-Aromatics-Resins-Asphaltenes) analysis on crude oil samples pre- and post-experiment (103 days) indicated a change in the mass fractions of the various components of crude oil after the application of low DC electrical field. The lighter compounds (e.g. saturates) were reported to increase, while the more complex compounds (e.g. asphaltenes) decreased, especially in the case of heavy crude oil (Ghazanfari, 2013).

Although the cited studies provide insight into the oil transformation due to an applied electrical field in porous media, the magnitude of viscosity change and its significance on flow needs further investigation. The gap in the literature in this area motivated this study. The main objective of this chapter was to use experimental and numerical tools to (i) investigate the feasibility of oil viscosity reduction due to applied electrical field; and more importantly, (ii) to investigate the significance of transient oil

viscosity on the flow during the oil recovery process. In the numerical investigation, EEOR is combined with water flooding and the generated two-phase immiscible flow under coupled pressure and electrical gradients for constant and transient values of oil viscosity are investigated. It should be noted that the focus of this chapter was not a detailed investigation of electrochemical reactions caused by application of DC electrical field that may result in the oil viscosity reduction, but rather the possibility of a such reduction and its effect on transport phenomena in two-phase immiscible flow during the oil recovery process.

The chapter is structured as follows: Section 4.2 provides the methodology and the results of the physical experiment. Section 4.3 presents the numerical experiment, which includes a brief description of the set of governing equations, the description of the numerical experiment set-up, and the results of the numerical simulation for different cases. The choice of cases was based on the transient viscosity correlation obtained in this chapter and those from reported laboratory and field applications in the literature. Finally, Section 4.3 provides conclusions based on the analysis of the obtained results.

## 4.2 PHYSICAL EXPERIMENT

In order to assess the feasibility of change in the oil viscosity due to application of low DC electrical field involved in EEOR method, a simple laboratory experiment was conducted. The experimental set-up and results are presented in the following section.

### 4.2.1 EXPERIMENTAL SET-UP

A synthetic formation was prepared in a cell as shown in Figure 4.2(a) to simulate

the EOR process. Sand (52.1% by mass), silt (39.8% by mass), kaolinite clay (8.1% by mass), brine with salinity of 33,000 ppm, and crude oil with initial dynamic viscosity of 2,800 cp and specific gravity of 0.95 at 20°C were mixed and packed into the test cell. The cylindrical test cell was 60 cm in length and 16 cm in diameter.

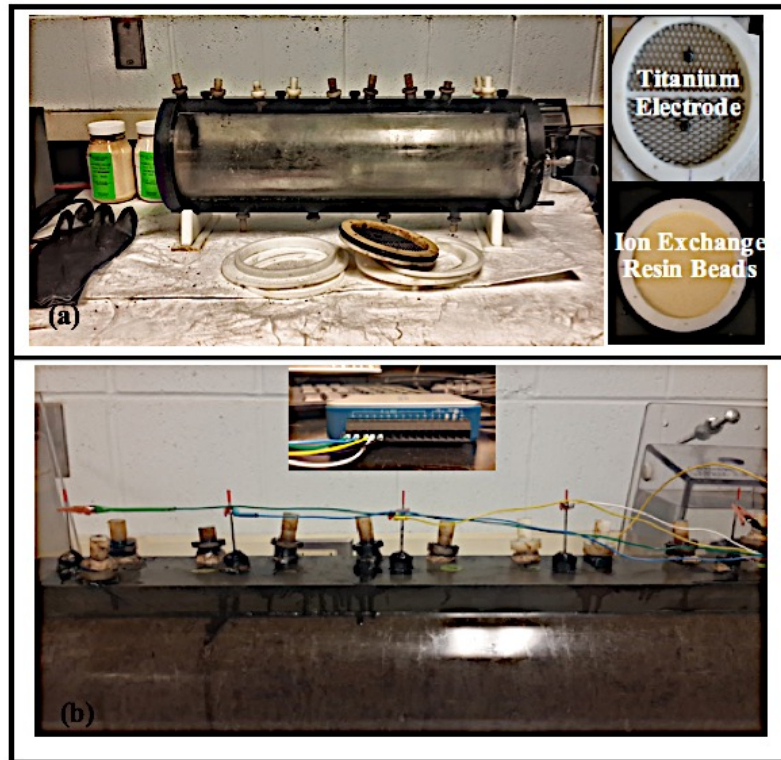


Figure 4.2: (a) Plexiglas test cell used in the experiment. The titanium electrode and the ion exchange resin beads are shown next to the cell (b) Wiring for the acquisition of voltage data (a picture of the DAQ is shown on the top center)

Extra care was taken to place a homogeneous and sufficiently compacted soil mixture into the cell. In order to achieve a well-compacted synthetic formation, the mixture was placed into the cell, which was kept in a vertical position during compaction, in layers of about 5 cm. After each layer was placed into the cell, it was compacted using a proctor. Once the mixture was packed, the cell was sealed and the initial porosity, water and oil

saturation of the synthetic formation was determined using weight volume relationships. The porosity of the synthetic formation was estimated as 0.34, and the brine and oil saturations were estimated as 45% and 55%, respectively. The test cell was placed horizontally for 24 hours to allow the internal fluids to uniformly distribute and equilibrate.

Titanium-mesh electrodes were placed at each end of the cell for application of the electrical field (Figure 4.2(a)). A pH control system was designed and installed adjacent to the electrodes. It consisted of a pack of weak base anion exchange resin (see Table 4.1 for properties) placed between the anode and the formation, and a pack of weak acid cation exchange resin placed between the cathode and the formation. In order to achieve good current conduction, the packs were kept saturated at all times with the same brine as was mixed with the soil inside the cell, using electrolyte reservoirs placed at each end. The pH control system aimed at limiting the electrolysis effect on the oil viscosity. Due to the electrolysis taking place at regions close to the electrodes, the viscosity change was expected to be enhanced in these regions. By placing the resin packs, the control region of the synthetic formation (i.e. region at the middle of the cell) was maintained at a neutral pH. This simulated the conditions in the oil reservoir away from the electrodes.

Table 4.1: Physical properties of the ion exchange resins used for pH control

Resin Type	Properties
Purolite A100 (Macroporous Weak Base Anion Exchange Resin)	<u>Polymer</u> - Macroporous crosslinked polystyrene divinylbenzene <u>Appearance</u> - Spherical beads <u>Functional Group</u> - Tertiary Amine
Purolite SST104 (Polyacrylic weak acid cation exchange resin)	<u>Polymer</u> - Porous crosslinked polyacrylic <u>Appearance</u> - Spherical Beads <u>Functional Group</u> - Carboxylic Acid

The hydraulic head was maintained constant (i.e. no head difference) by keeping the electrolyte elevations constant in both the anode and cathode electrolyte reservoirs throughout the experiment. This assured minimal flow due to a hydraulic gradient. The test cell was placed in a horizontal position to eliminate flow due to gravity. Despite the precautions taken, after 10 days of low DC electrical field application (i.e. current density =  $0.1 \text{ A/m}^2$ ), oil was observed in the electrolyte reservoir connected to the cathode, while no oil was present in the anode reservoir. Although diffusion could take place, the fact that oil was only observed in the cathode reservoir might be an indication of flow due to the application of the electrical field. The temperature of the room remained relatively constant ( $\sim 22^\circ\text{C}$ ) during the two-month period that the experiment was underway. The experimental set-up is shown in Figure 4.3(a).

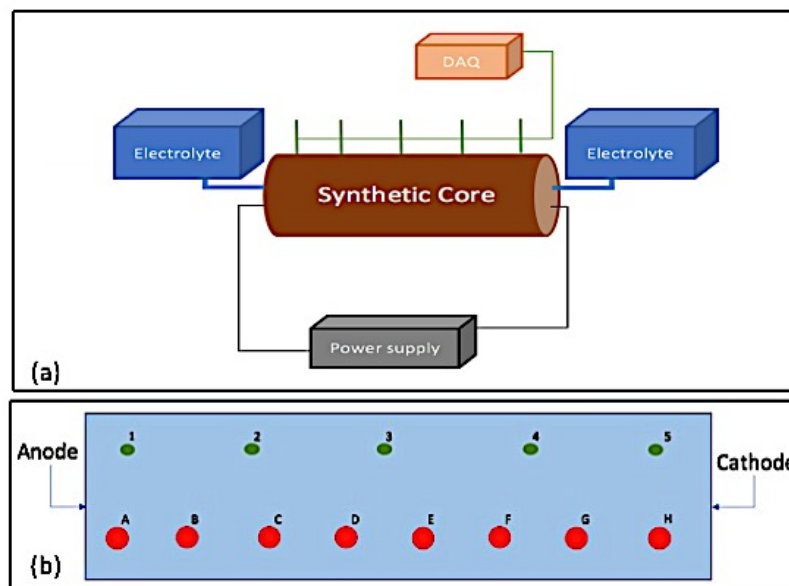


Figure 4.3: (a) Schematic of the experimental set-up (b) Ports used for data collection (green (1-5): voltage data collection; red (A-H): pH and ORP data collection)

#### 4.2.2 EXPERIMENTAL DATA AND RESULTS

Stainless steel probes for voltage measurements were inserted into the test cell using 5 ports (see Figure 4.3(b)) and connected using wires to a data acquisition (DAQ) device (see Figure 4.2(b)). In order to monitor the fluctuations of the electrical field, a LabView code was used to record the applied voltage for every hour of the 2-month long experiment. The total applied voltage was maintained at around 18 Volt (i.e. voltage gradient of 0.3 Volt/cm) with a current density of  $0.1 \text{ A/m}^2$ . The voltage gradient at the center of the cell (ports 3 and 4), the region of interest for our analysis, is shown in Figure 4.4, and appears to be relatively constant. After the first month of the experiment, the voltage gradient appeared to increase slightly. This is most probably due to sampling for

the viscosity measurement, a process that changed the equilibrium of the system because of the removed soil mixture from the middle region of the cell.

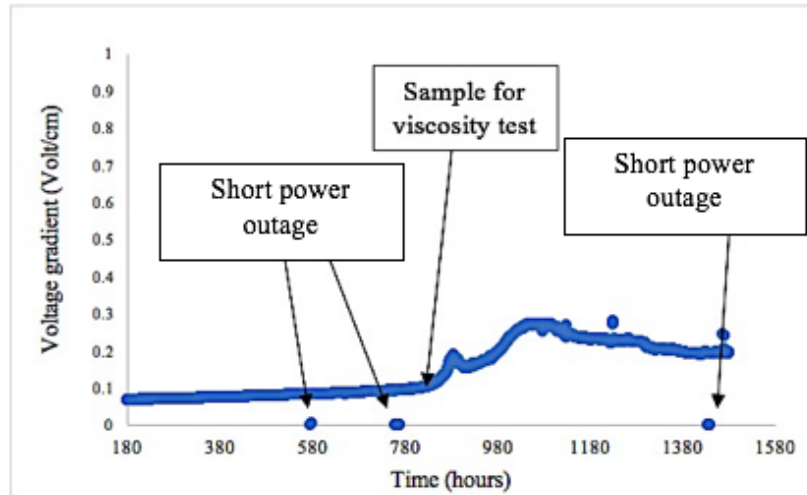


Figure 4.4: Voltage gradient at the center of the cell (Ports 3 and 4)

Throughout the experiment, small samples of the soil mixture were extracted from 8 ports located across the length of the cell (Figure 4.3(b)) to measure the oxidation-reduction potential (ORP) and the pH of the mixture. The ORP measurements served as an indication of electrochemical reactions taking place in the synthetic formation, and the pH measurements were employed to indicate the need to replace the resin packs throughout the experiment. The ORP values changed about 100-120% at the regions close to the electrodes, and 50-70% in the center region. This might be attributed to the electrochemical reactions, and their results on the crude oil viscosity are presented in the following section. The value of pH dropped from 7 to 5.8 at the anode region, from 7 to 6.5 at the center region, and increased from 7 to 10.5 at the cathode region, as shown in Figure 4.5.

It should be noted that the pH in the center region (Ports C and D in Figure 4.3(b)) was indeed maintained close to the initial pH value (Figure 4.5). An indication of occurrence of electrolysis reactions at the regions close to the electrodes was the change in the pH. It was impossible to control the pH in these regions, even after replacement of the resin packs at 25 days. The pH at the center region remained relatively constant at a value of about 7.

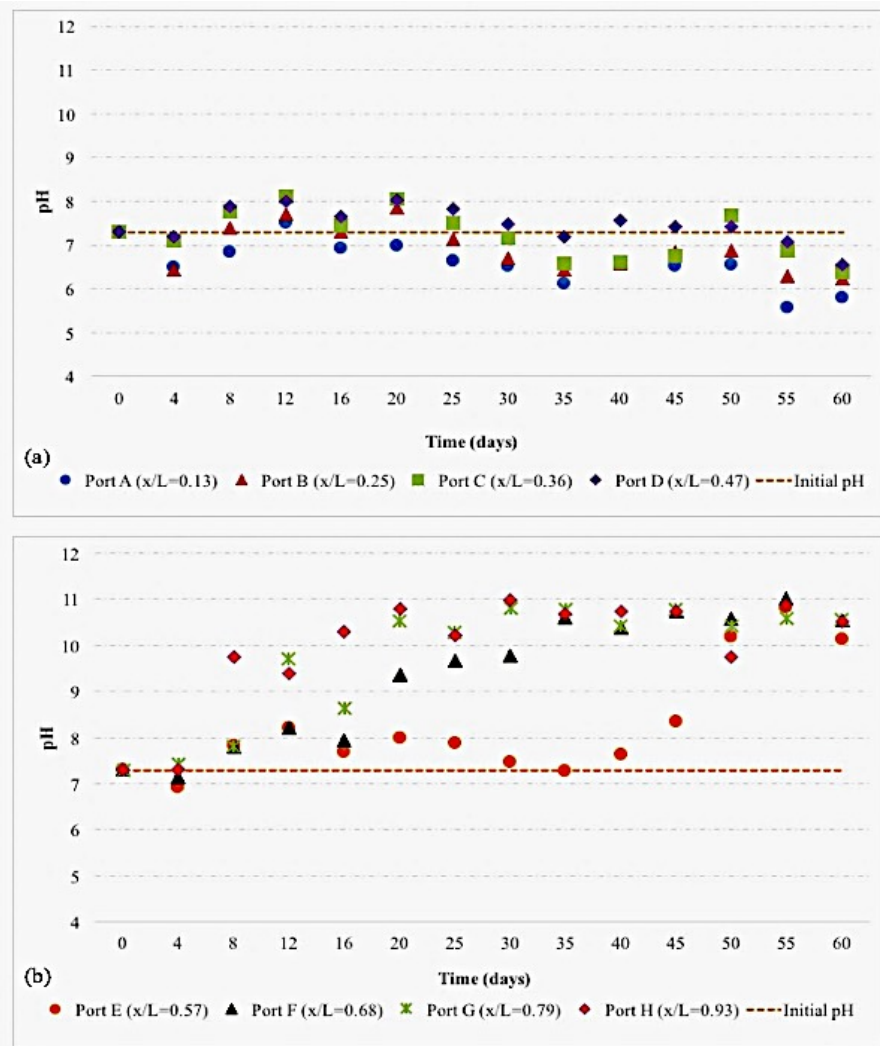


Figure 4.5: Measured pH at: (a) the ports closer to the anode and (b) the ports closer to the cathode.  $x$  is the distance from the anode and  $L$  the total length of the cell (60 cm)

A sample was taken from the initial soil mixture (i.e. before applying electrical field), a second sample from the center region of the synthetic formation after 1 month of continuous electrical field application, and a third sample from the center region at the end of the two-month experiment. The crude oil was retrieved from these samples using a centrifuge rotating at 5,000 rpm for 5 hours which separated the oil from the soil and the brine. Only the center region was selected for sampling because: (i) it was considered the important region to examine as it was located furthest away from the electrodes where electrolysis took place; (ii) due to difficulties involved in the process of extracting soil sample out of the synthetic formation through small ports; and (iii) concerns that the extraction of additional soil would cause a void space in the formation that could disturb the balance of the system and cause movement of fluids to fill the void. The dynamic viscosity measurements (using DHR3 rheometer) at room temperature on the collected oil samples from the center region indicated approximately a 6% reduction after one month and a 17% reduction after 2 months of electrical field application.

It should be noted that limitations in the experimental procedure, such as uniformity of the soil mixture and the small voids formed in the mixture caused by sampling, may not exactly reflect the reality in the EOR application. However, the slight change observed in the viscosity of the crude oil in the center region of the test cell motivated a numerical modeling study of the significance of transient viscosity change on two-phase immiscible flow in the EOR method. This is presented in the following section.

### 4.3 NUMERICAL EXPERIMENT

As mentioned in Section 4.1, the EOR method is usually combined with waterflooding in the field. In this section, a numerical experiment is set up for a hypothetical reservoir to examine the effect of the transient oil viscosity (caused by the applied electrical field) on the two-phase flow in the EOR method. In order to gain insight into the importance of oil viscosity in transport phenomena during oil production using the EOR method, the governing equations are presented in this section. These equations formed the foundation for the design of the numerical model used in this chapter. More details about the derivation of the governing equations, assumptions, solution scheme, and model sensitivity to various parameters can be found in Chapter 3.

#### 4.3.1 GOVERNING EQUATIONS

The equations describing the two-phase flow (water (w) and oil (o)) in the EOR method are (Ghazanfari and Pamukcu, 2014; Peraki et al., 2017):

$$\frac{\partial(\varphi S_w)}{\partial t} - \nabla \cdot (\mathbf{f}_w \cdot \nabla P) - \nabla \cdot (k_{er,ww} \mathbf{k}_{eo} \cdot \nabla \Phi) = \frac{q_w}{\rho_w} \quad (4.1)$$

$$\frac{\partial(\varphi S_o)}{\partial t} - \nabla \cdot (\mathbf{f}_o \cdot \nabla P) - \nabla \cdot (k_{er,wo} \mathbf{k}_{eo} \cdot \nabla \Phi) = \frac{q_o}{\rho_o} \quad (4.2)$$

where,  $\varphi$  is the porosity of the porous medium,  $\rho_\alpha$  is the density of the phase  $\alpha$ ,  $S_\alpha$  is the saturation of phase  $\alpha$ ,  $\mathbf{f}_\alpha$  is the fractional flow of phase  $\alpha$  (see Eq. 4.3),  $P$  is the global pressure,  $\mathbf{k}_{eo}$  is the electro-osmotic permeability coefficient of the medium,  $k_{er,ww}$  and  $k_{er,wo}$  are the relative electro-osmotic permeability coefficients,  $\Phi$  is the applied electrical

potential, and  $q_\alpha$  is the source/sink term. The fractional flow of each phase is defined as (Dake, 1978; Arnes, et al., 2007):

$$\mathbf{f}_\alpha = \boldsymbol{\lambda}_\alpha \cdot (\boldsymbol{\lambda}_{\text{tot}})^{-1} \quad (4.3)$$

where,  $\boldsymbol{\lambda}_\alpha$  is the mobility of phase  $\alpha$  and  $\boldsymbol{\lambda}_{\text{tot}}$  is the sum of the phase mobilities:

The phase mobility is defined as (Dake, 1978; Arnes, et al., 2007):

$$\boldsymbol{\lambda}_\alpha = \frac{\mathbf{K} k_{r\alpha}}{\mu_\alpha} \quad (4.37)$$

where,  $\mathbf{K}$  is the absolute permeability tensor of the porous medium,  $k_{r\alpha}$  is the relative permeability of phase  $\alpha$ , and  $\mu_\alpha$  is the dynamic viscosity of phase  $\alpha$ .

The global pressure is calculated using (Ghazanfari and Pamukcu, 2014; Peraki et al., 2017):

$$-\nabla \cdot [\boldsymbol{\lambda}_{\text{tot}} \cdot \nabla P + \mathbf{k}_{\text{eo}} \cdot (k_{\text{er},\text{ww}} + k_{\text{er},\text{wo}}) \cdot \nabla \Phi] = \frac{q_w}{\rho_w} + \frac{q_o}{\rho_o} \quad (4.5)$$

By examining Eqs. 4.1 and 4.5, we notice that a potential change in the oil viscosity over time, due to the application of the electrical field, can be incorporated into the solution for saturation and pressure equations through the mobility of the oil phase that depends on the viscosity of the phase (Eq. 4.4). The mobility of the oil phase, although not obvious in Eqs. 4.1 and 4.5, is included in the  $\mathbf{f}_w$  and  $\boldsymbol{\lambda}_{\text{tot}}$  terms.

For the calculation of the applied electrical potential, Ohm's law is used (Avants, et al., 1999; Alshawabkeh, 2001):

$$\nabla \cdot \mathbf{i} = \frac{1}{\rho} \nabla \cdot \mathbf{E} \quad (4.6)$$

where  $\mathbf{i}$  is the applied current density,  $\rho$  is the average resistivity of the reservoir, and  $\mathbf{E}$  is the applied electrical gradient ( $\nabla\Phi$ ).

Since the current density is maintained constant during EEOR field applications (Wittle et al., 2008; Hill, 2014), we have:

$$\nabla \cdot \mathbf{E} = -\nabla^2\Phi = 0 \quad (4.7)$$

To complete Eqs. 4.1, 4.5, and 4.7, proper initial and boundary conditions must be prescribed.

A cell-centered finite volume scheme, also referred to as the two-point flux approximation (Arnes, et. al., 2007; Khattri, 2007), was used for the discretization of the water saturation and pressure equations. The Implicit-Pressure-Explicit-Saturation (IMPES) method was used to solve the pressure and saturation equations. Using this method, the pressure was advanced implicitly in time and the saturation was updated explicitly. Because we solved the saturation explicitly, we imposed a stability condition, which is called the Courant-Friedrichs-Lewy (CFL) condition, on the time step (Aziz and Settari, 1979; Chen, et al., 2004).

#### 4.3.2 NUMERICAL EXPERIMENT SET-UP

A system of one injection well and one production well placed in opposite corners of a hypothetical two-dimensional sandstone reservoir was used in the numerical experiment (Figure 4.6). The selected parameters for the reservoir were taken from reasonable ranges available in the literature and are presented in Table 4.2 (Brooks and Corey, 1964; Okandan, 1984; Bassiouni, 1994; Alshawabkeh, 2001; Christle and Blunt, 2001; Sadikh-Zadeh, 2006; Wittle and Hill, 2006; Arnes, et al., 2007; Wittle, et al., 2011; Ghazanfari, et al., 2014; Chillingar and Haroun, 2014). The grid consisted of square cells with dimensions of  $60 \times 120 \times 1$  grid-blocks, with 7,200 cells in total. For the pressure equation (Eq. 4.5), no-flow boundary conditions around the reservoir were imposed (Aziz and Settari, 1979; Chen, et al., 2006; Arnes, et al., 2007). Typically for field applications of the EOR method, the current density is maintained constant and no flow of electrical current is assumed through the boundaries of the examined reservoir (Avants, et al., 1999; Alshawabkeh, 2001).

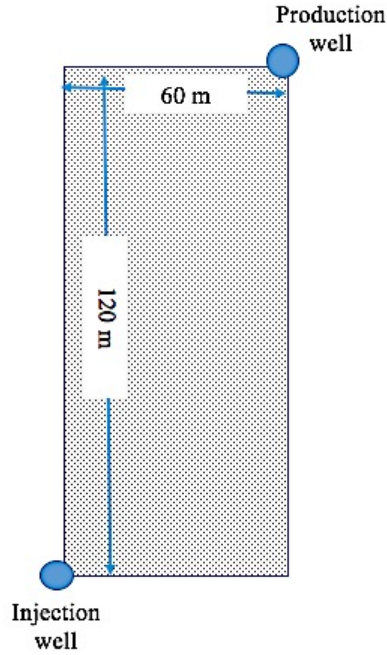


Figure 4.6: Schematic of the 2D reservoir used in simulation

Table 4.2: Characteristics of reservoir used in numerical simulation

Parameter	Value
Dimensions of reservoir	60 m × 120 m
Porosity	0.2
Absolute permeability	100 mD
Absolute electro-osmotic permeability	$1 \cdot 10^{-9} \text{ m}^2/(\text{Volt} \cdot \text{sec})$
Viscosity of water	$3 \cdot 10^{-4} \text{ kg}/(\text{m} \cdot \text{s})$
Irreducible oil saturation	0.2
Connate water saturation	0.2
Initial water saturation	0.4
Initial oil saturation	0.6
Injection rate	$9.15 \text{ m}^3/\text{day}$
Salinity of water phase	$0.5 \text{ } \Omega \cdot \text{m}$

To verify the sensitivity of the model to oil viscosity, the cumulative oil production (i.e. the gross amount of oil produced over a time period) was calculated under different scenarios of oil viscosity and the results are presented in Figure 4.7. The total simulation period was set to 300 days with a global time step of 1 day. Each global time step was solved as many times (local time steps) as required to maintain the stability of the solution (Eq. 4.1). The applied current density to the reservoir was set at  $1 \text{ A/m}^2$  for all scenarios. As it can be seen from Figure 4.7, the cumulative oil production decreased as the value of oil viscosity increased, because of the effect of oil viscosity on the mobility of the oil phase. As expressed in Eq. 4.4, the mobility of the oil phase increases as the oil viscosity decreases.

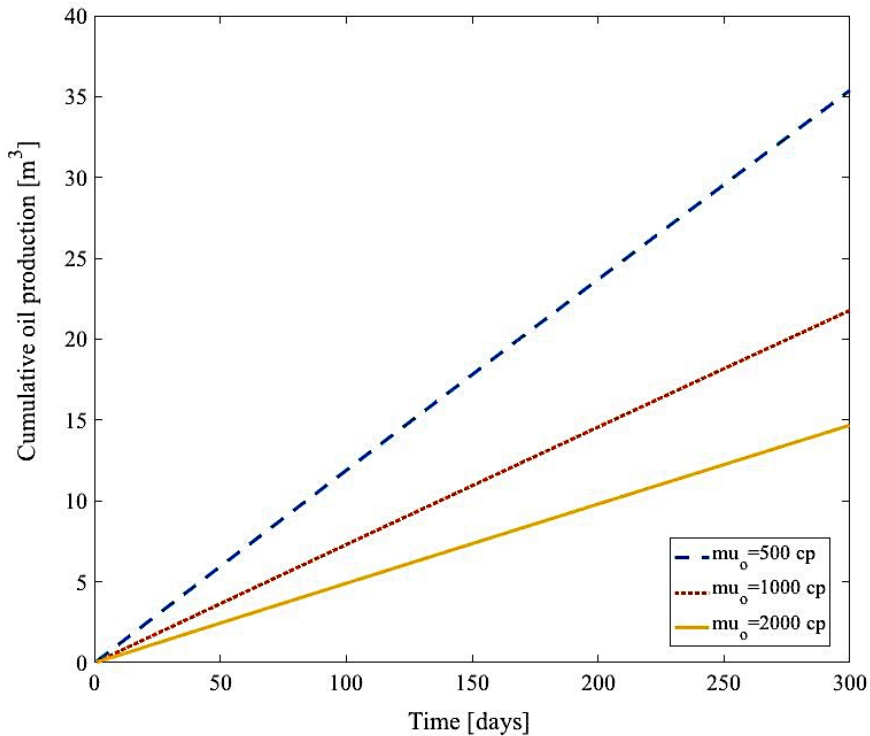


Figure 4.7: Results of numerical simulation for cumulative oil production for different values of oil viscosity

In the above examined cases, the viscosity of the crude oil was assumed to be constant at all times. In the following section, the effect of transient changes in the oil viscosity (caused by applied electrical field) on the transport phenomena was investigated. It should be mentioned that the effects of temperature and pressure on viscosity change were not incorporated in the numerical experiment since the main focus of this study was the effect of the electrochemical reactions due to the applied electrical field.

#### 4.3.3 RESULTS OF NUMERICAL EXPERIMENT

In an effort to examine the significance of the oil viscosity reduction on the flow under different scenarios such as applied current density, initial oil viscosity, and scale of the application, the data obtained from the physical experiment presented in Section 4.2 and available experimental and field data from the literature were used for the numerical experiment. The temporal change in the oil viscosity under the applied electrical field was represented using a linear interpolation equation, and its significance on flow (e.g. cumulative oil production) was investigated in different cases.

##### Case I

The oil viscosity values obtained from the center of the cell in the physical experiment presented in Section 4.2. (i.e. initial viscosity, after 1 month, and a final viscosity after 2 months) were used to create a linear interpolation of the change in viscosity with time under an applied electrical field. It should be emphasized that the resulting linear interpolation equation was specific to the test conditions.

A numerical simulation was performed for two scenarios of constant and transient

oil viscosity using the above-mentioned relationship. The total simulation period was set to 60 days with a global time step of 1 hour for the hypothetical reservoir. The results of the simulation are presented in Figure 4. 8. At the beginning of the simulation, the cumulative production curves matched for the two scenarios, however, the two curves started to diverge after about 20 days. The effect of the gradually decreased oil viscosity on the transport phenomena became more profound as time progressed until the end of the simulation. The total oil production increased by about 6% due to the temporal decrease in the oil viscosity. The simulation was limited to 60 days (duration of physical experiment) to reflect the timing from physical experiment.

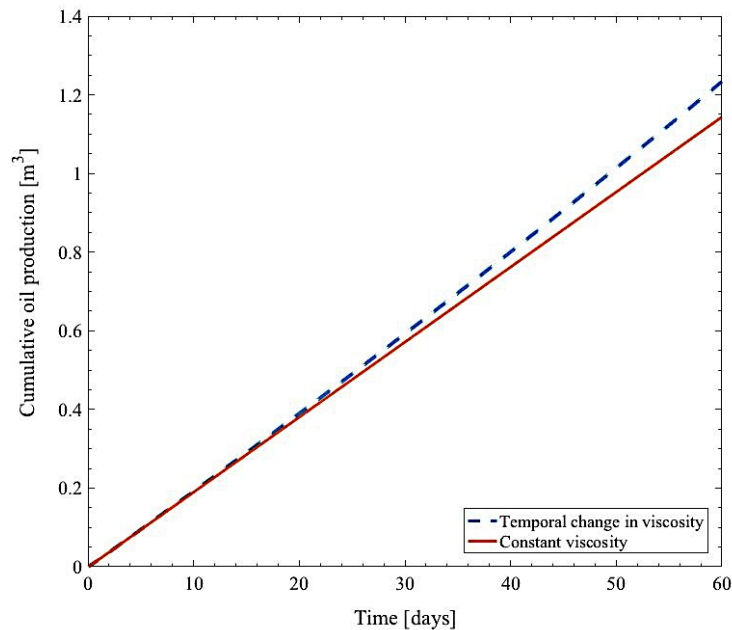


Figure 4. 8: Results of numerical simulation using experimental data presented in Section 4.2. The applied current density is  $0.1 \text{ A/m}^2$  and the initial oil viscosity is 2,800 cp.

## Case II

Ghazanfari (2013) reported results of an experimental study on a synthetic formation, where current density of  $0.78 \text{ A/m}^2$  was applied for 102 days to the formation. The initial oil viscosity was 97 cp, and was reported to decrease to 74 cp after 102 days of electrical field application. A linear equation for viscosity change with time based on this information and specific to this case was developed. The results of the numerical simulation using this information (i.e. current density of  $0.78 \text{ A/m}^2$ ; time: 102 days; developed linear equation for viscosity change) for the hypothetical reservoir are presented in Figure 4.9.

At the beginning of the simulation, the cumulative production curves matched for the two scenarios (i.e. constant and transient viscosity), but the two curves started to diverge after about 30 days. The total cumulative oil production increased by about 10% due to the change in the viscosity. The effect of the viscosity change was more evident for the lighter crude oil (initial viscosity of 97 cp) in this case than the heavy crude oil used in the physical experiments presented in Section 4.2. This might be attributed to the already higher mobility of the lighter oil compared to the mobility of the heavier crude oil. A further decrease in the viscosity, caused by the applied electrical field, enhanced the already higher mobility of the oil phase.

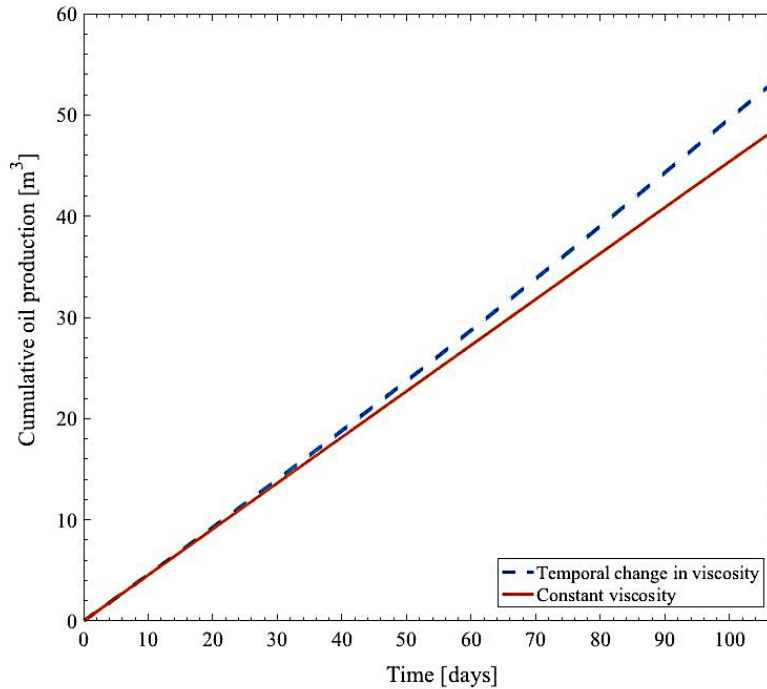


Figure 4.9: Results of numerical simulation using experimental data from Ghazanfari, 2013 (light crude oil). The applied current density is  $0.78 \text{ A/m}^2$  and the initial oil viscosity is 97 cp.

### Case III

Wittle et al., 2008 reported the EOR laboratory experiment results on a synthetic formation (1m x 1m x 1m) that was impregnated with crude oil (viscosity of 2,635 cp) and brine. A current density of  $1 \text{ A/m}^2$  was applied for 60 days to the formation. The final viscosity value was reported to be around 1,200 cp. The results of the numerical simulation using this information (i.e. current density of  $1 \text{ A/m}^2$ ; time: 60 days; developed linear equation for viscosity change using viscosity measurements at seven times intervals during the experiment) for the hypothetical reservoir are presented in Figure 4.10.

Notice how the initial viscosity was close to that for the case presented in Figure 4.8, but the applied current density was one order of magnitude higher. This increase in current density might have enhanced the process of viscosity reduction. It should be noted that higher current density will likely lead to a wider zone of electrolysis reaction close to the electrodes where the oil viscosity decreases to a greater extent, but that does not represent most regions of the reservoir. The two curves (constant and varying value of oil viscosity) for cumulative oil production, exhibited a similar trend with the two previous cases, however, the increase in cumulative oil production was more evident in this case reaching to about 20 % (Figure 4.10).

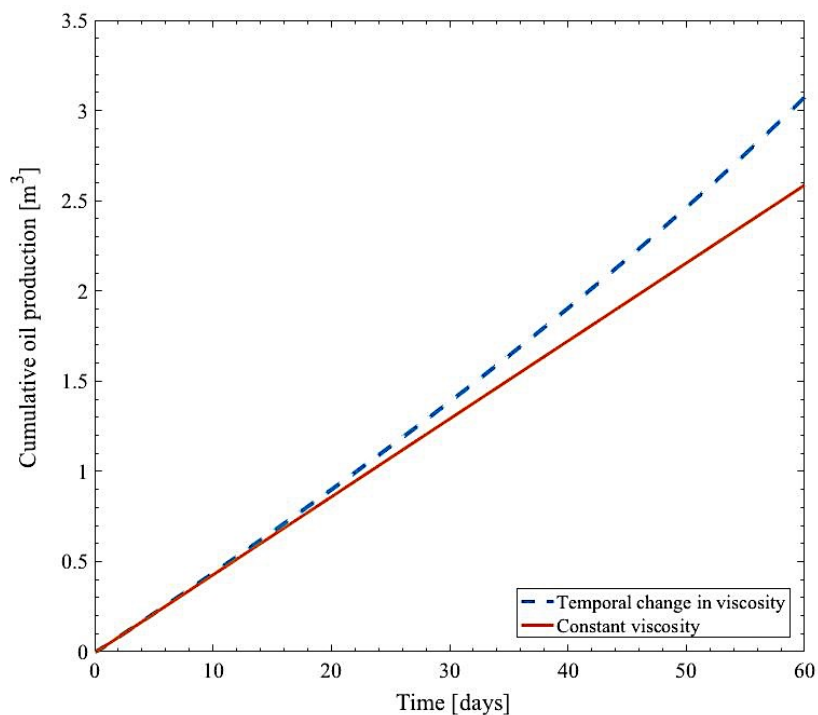


Figure 4.10: Results of numerical simulation using experimental data from Wittle et al., 2009. The applied current density is  $1 \text{ A/m}^2$  and the initial oil viscosity is 2,635 cp.

#### Case IV

This case involved using data from a field application of the EEOR method in the Golfo San Jorge Basin (Santa Cruz, Argentina) reported by Hill (2014). The total field test duration was 51 days. The initial oil viscosity was reported at 2,854 cp and the final value of oil viscosity at 640 cp, meaning that the value was reduced by 77.5 %. In this field application, oil samples were taken primarily from the production wells (close to the cathode). The reported drastic change in the viscosity could be attributed to the electrolysis of the brine close to the electrodes, enhancing the electrochemical reactions that reduce the oil viscosity (Wittle et al., 2008; Hill, 2014).

The results of the numerical simulation using this information (i.e. current density of 1 A/m<sup>2</sup>; time: 51 days; developed linear equation for viscosity change) in the hypothetical reservoir are presented in Figure 4.11. The dramatic decrease of the oil viscosity resulted in 84% increase in the oil production. As it can be seen from Figure 4.11, the two curves started diverting after only 10 days, and the curve that incorporated the transient change in the oil viscosity demonstrated a steep upward slope due to the rapid change of the oil viscosity, and therefore of the oil mobility.

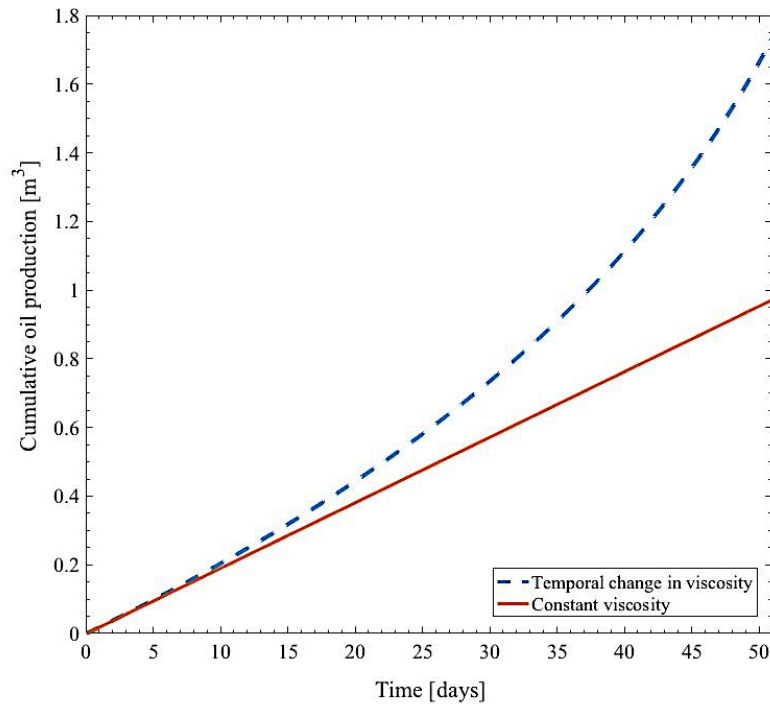


Figure 4.11: Results of numerical simulation using field data from Golfo San Jorge Basin (Hill, 2014). The applied current density is  $1 \text{ A/m}^2$  and the initial oil viscosity is  $2,854 \text{ cp}$

#### 4.4 SUMMARY

This chapter investigated the reduction in the oil viscosity due to application of the electrical field involved in the EOR method and the significance of this reduction to the transport phenomena that take place during the oil recovery process. A physical experiment was carried out to investigate the phenomenon of oil viscosity change due to application of an electrical field, which indicated slight reduction in the oil viscosity at the center region of the test cell.

To examine the effect of the temporal change in the oil viscosity on the transport phenomena, and therefore on the oil production, a numerical experiment was performed.

The data from the conducted experiment and from other experimental and field applications available in the literature were used to approximate the value of the oil viscosity with time using a linear equation. The results of the numerical experiment indicated that incorporating the transient changes in the oil viscosity leads to a considerable increase in the cumulative production. As expected, the higher the reduction of oil viscosity due to electrical field application, the more evident the increase in the cumulative oil production was. It should be noted that further research on the electrochemical reactions and their effect on transport phenomena during oil recovery is needed. Future work may include effects of pressure and temperature on viscosity changes, improvements in the design of the field experiments (e.g. type of measurements, timing of sampling) in order to obtain useful data for calibration of numerical models and further investigation of the underlying mechanisms involved in the EEOR method.

## CHAPTER 5

### CONCLUSIONS AND FUTURE WORK

In this dissertation, application of electrokinetic phenomena in subsurface energy extraction was investigated. Electrodialysis was studied at laboratory scale as a method of pre-treatment of the flow-back water produced during fracturing stage of shale gas extraction. In addition, the electrically assisted oil recovery was investigated experimentally and numerically as a potential technique for the enhancement of oil extraction, especially for the case of heavy crude oil.

The main conclusions of this dissertation are:

1. Electrodialysis was found to be a relatively effective method for TDS level reduction of flow-back water. Using  $\text{Na}_2\text{SO}_4$  or  $\text{NaCl}$  solution as electrolyte, the maximum TDS level reduction was found to be about 27% after 7 hours of low direct current electric field application. The parameter that affected the results the most was found to be the duration of the electrical field application. The magnitude of the applied current seemed to play a secondary role. However, an intermediate value of applied current is a better choice to overcome the effect of the diffusion of the ions through the membranes. The type of the electrolyte, the concentration of the electrolyte and the range of the initial concentration did not cause a statistically significant difference in the results. However,  $\text{NaCl}$  as an electrolyte presented a steadier and more consistent performance than  $\text{Na}_2\text{SO}_4$ .

2. A numerical experiment was designed to evaluate the importance of different parameters involved in electrically enhanced oil recovery (EEOR) combined with water flooding. A sensitivity analysis was performed to examine the sensitivity of the developed model to various reservoir parameters and then to evaluate the importance of field operational parameters. In addition, the direct contribution of the applied electrical field to the flow (i.e. oil production) was investigated.

The sensitivity analysis showed that porosity, absolute electro-osmotic permeability, relative permeability of water and of oil, initial water saturation, oil viscosity, applied current density, water resistivity, and water injection rate are important parameters affecting oil production using this method. Parameters such as relative electro-osmotic permeability and absolute permeability were not found to have a significant effect for the examined problem. In addition, it was found that the applied electrical gradient involved in EEOR combined with the water flooding method contributed to a very small increase in oil production.

3. A physical experiment was carried out to investigate the phenomenon of oil viscosity change due to application of an electrical field. The results of the experiment indicated a slight reduction in the oil viscosity at the center region of the test cell.

To examine the effect of the temporal change in the oil viscosity on the transport phenomena, and therefore on the oil production, a numerical experiment was performed. The data from the conducted experiment and from other experimental and field applications available in the literature were used to approximate the value of the oil viscosity at each time step using a linear equation. The results of the numerical experiment

indicated that incorporating the transient changes in the oil viscosity leads to a considerable increase in the cumulative oil production.

Some suggestions for future work are:

- A numerical simulation of the phenomena involved in the electro dialysis method would reinforce the results of the statistical analysis presented in Chapter 2. A numerical model would allow the realization of multiple trials whose results could be used for a more in depth analysis of the efficiency of the method.

- Additional experiments should be performed to better understand the effect of the EEOR method on the crude oil viscosity. Further analysis on the composition of the heavy crude oil before, during, and after the experiments could shed light on the reasons for the reduction of the crude oil viscosity.

- In order to achieve a more detailed analysis of the viscosity reduction phenomena, the sampling method for viscosity measurements should be improved. For this dissertation, the samples were collected through narrow ports using a drill head, a method that did not allow more samples being extracted. In addition, the effect of pressure and temperature on the oil viscosity should be incorporated in the numerical model to improve the model predictions.

- A continuous power supply should be used to ensure the uninterrupted application of the electrical field and allow the continuous monitoring of the applied voltage gradient using the DAQ.

- Data from field application of EEOR method are essential for the calibration of the developed numerical model. Although a sensitivity analysis was performed, the

calibration of the model is vital for further validation of its results. After the calibration, the model could be used for the investigation of the EEOR in future field application.

- Finally, an important parameter that affects the efficiency of the EEOR method is the configuration of the electrodes. The numerical code developed in Chapter 3 is not capable of comparing different configurations due to the use of Laplace equation for the calculation of the voltage distribution. There are, however, additional numerical approaches that can incorporate electrodes placed in different positions. After different configurations have been tested numerically, evaluation of the results could improve the efficiency of the method in the field application.

## BIBLIOGRAPHY

- Abdalla, C.W., Drohan, J.R., Saacke Blunk, K., and Edson, J.. (2011). Marcellus Shale Wastewater Issues in Pennsylvania-Current and Emerging Treatment and Disposal Technologies. Technical Report, Penn State Extension, College of Agricultural Sciences.
- Abramson, H. A.. (1934). Electrokinetic phenomena and their application to biology and medicine. *Journal of Physical Chemistry*, Volume 38(8), pp. 1128-1129.
- Acar, Y.B., and Alshawabkeh, A.N.. (1993). Principles of electrokinetic remediation. *Environmental Science and Technology*, Volume 27(13), pp. 2638–2647.
- Acar, Y. B., Alshawabkeh, A. N., and Parker, R. A.. (1997). Theoretical and experimental modeling of multi-species transport in soils under electric fields. Technical report. EPA/600/R-97/054.
- Aggour, M. A., and Muhammadain, A. M.. (1992). Investigation of waterflooding under the effect of electrical potential gradient. *Journal of Petroleum Sciences and Engineering*, Volume 7, pp. 317-327.
- Ahmadun, F.R., Pendashteh, A., Abdullah, L.C., Awang, D.R., Madaeni, S.S., and Abidin, Z.Z.. (2009). Review of technologies for oil and gas produced water treatment. *Journal of Hazardous Materials*, Volume 170, pp. 530-551.
- Al Shalabi, E. W., Haroun, M., Ghosh, B., and Pamuksu, S.. (2012a). The stimulation of sandstone reservoirs using DC potential. *Petroleum Science and Technology*, Volume 30, pp. 2137-2147.
- Al Shalabi, E. W., Haroun, M., Ghosh, B., and Pamuksu, S.. (2012b). The application of direct current potential to enhancing waterflood recovery efficiency. *petroleum Science and Technology*, Volume 30, pp. 2160-2168.
- Al-Khlaifat, A., and Arastoopour, H.. (2001). Simulation of Two-Phase Flow Through Anisotropic Porous Media. *Journal of Porous Media*, Volume 4 (4), pp. 1-8.
- Alshawabkeh, A.N., and Acar, Y.B.. (1996). Electrokinetic Remediation: II. Theory. *Journal of Geotechnical Engineering*, ASCE, Volume 122 (3), pp. 186-196.
- Alshawabkeh, A.. (2001). Basics and applications of electrokinetic remediation (short-course handout). Rio de Janeiro, Brazil.
- Amba, S. A., Chillingar, G. V., and Beeson, C. M.. (1964). Use of direct electrical current for increasing the flow rate of reservoir fluids during petroleum recovery. *Journal of Canadian Petroleum Technology*, Volume 3, pp. 8-14.

- Amba, S. A., Chillingar, G. V., and Beeson, C. M.. (1965). Use of direct current for increasing the flow rate of oil and water in a porous medium. *Journal of Canadian Petroleum Technology*, Volume 4, pp. 81-88.
- Archie, G. E.. (1942). Electrical resistivity log as an aid in determining some reservoir characteristics. *Petroleum Transactions of AIME*, Volume 146, pp. 54-61.
- Arnes, J. E., Gimse, T., and Lie, K.-A.. (2007). An introduction to the numeric of flow in porous media using Matlab. Eds. Hasle, G., Lie, K., and Quak, E.. In: *Geometrical modeling, numerical simulation and optimization: industrial mathematics at SINTEF*. Berlin: Springer-Verlag.
- Arthur, D.J.. (2011). Management of produced water from oil and gas wells. Working document of the NPC North American Resource Development Study Report.
- Avants, B., Soodak, D., and Ruppeiner, G.. (1999). Measuring the electrical conductivity of the earth. *American Journal of Physics*, Volume 67(593).
- Aziz, K., and Settari, A.. (1979). *Petroleum reservoir simulation*. London: Applied Science Publishers LTD.
- Bai, W., Kong, L., and Guo, A.. (2013). Effects of physical properties on electrical conductivity of compacted lateritic soil. *Journal of Rock Mechanics and Geotechnical Engineering*, Volume 5, pp. 406-411.
- Banasiak, L.J., Kruttschnitt, T.W., and Schafer, A.I.. (2007). Desalination using electro dialysis as a function of voltage. *Desalination*, Volume 205, pp. 38-46.
- Bassiouni, Z.. (1994). *Theory, measurement, and interpretation of well logs*. Society of Petroleum Engineers.
- Bauer, D., Goyeau, B., and Gobin, D.. (2008). Large Particle Transport in Porous Media: Effect of Pore Plugging on the Macroscopic Transport Properties. Volume 11(4), pp. 343-360.
- Bazinet, L., Lamarche F., and Ippersie, D.. (1998). Bipolar-membrane electro dialysis: Applications of electro dialysis in food industry. *Trends in Food and Science Technology*, Volume 9, pp. 107-113.
- Bear, J., and Yehuda, B.. (1990). *Introduction to modeling of transport phenomena in porous media*. Dordrecht: Kluwer Academic Publishers.
- Bientinesi, M., Petarca, L., Cerutti, A., Bandinelli, M., De Simoni, M., Manotti, M., and Maddinelli, G.. (2013). A radiofrequency/microwave heating method for thermal heavy oil recovery based on a novel tight-shell conceptual design. *Journal of Petroleum Science and Engineering*, Volume 107, pp. 18-30.

- Bishop, W.F., and Murphy, M.. (1972). Electrodialysis. American Water Works Association, Volume 64 (11), pp. 783-785.
- Brooks, R. H., and Corey, A. T.. (1964). Hydraulic properties of porous media. Fort Collins, CO: Colorado State University.
- Bruell, C.J., Segal, B.A., and Walsh, M.T.. (1992). Electroosmotic removal of gasoline hydrocarbons and TCE from clay. Journal Environmental Engineering ASCE, Volume 118(1), pp. 63–68.
- Cassagrande, L.. 1952. electroosmotic stabilization of soil. Journal of Boston Society of Engineers, Volume 39, pp. 258-317.
- Castle, J.W., Rodgers, J.H., Jr., Alley, B., Beebe, A., Coffey, R., Jurinko, K., Pardue, M., Ritter, T., and Spacil, M.M.. (2013). Innovative Water Management Technology to Reduce Environmental Impacts of Produced Water. Clemson University, SC.
- Chavent, G., and Jaffre, J., 1986. Mathematical models and finite elements for reservoir simulation. Amsterdam, The Netherlands: Elsevier Science Publishers B.V.
- Chen, Z., Huan, G., and Li, B.. (2004). An improved IMPES method for two phase flow in porous media. Transport in porous media, Volume 54 (3), pp. 361-376.
- Chen, Z., Huan, G., and Ma, Y.. (2006). Computational methods for multiphase in porous media. Society of Industrial and Applied Mathematics.
- Chillingar, G. V., Adamson, C. G., Riene, H. H., and Grey, R. R.. (1968). Electrochemical treatment of shrinking soil. Engineering Geology, Volume 2, pp. 197-203.
- Chillingar, G. V., and Haroun, M.. (2014). Electrokinetics for Petroleum and Environmental Engineers. Salem(Massachusetts): Scrivener Publishing LLC and John Willey & Sons, Inc.
- Christle, M. A., and Blunt, M. J.. (2001). Tenth SPE comparative solution project: A comparison of the upscaling techniques. SPE, 72469. URL: [www.spe.org/csp](http://www.spe.org/csp).
- Civan, F.. (2011). Porous media transport phenomena. Hoboken, NJ: John Wiley & Sons, Inc.
- Dake, L. P.. (1978). Fundamentals of reservoir engineering. Amsterdam, The Netherlands: Elsevier Science B.V.
- Electorowicz, M.. (2009). Electrokinetic remediation of mixed contaminated soils. Chapter 15 in Electrochemical Remediation Technologies for Polluted Soils, Sediments and Groundwater, eds. Reddy and Camaselle; John Wiley & Sons.

- Ferre, P. A., Redman, J. D., and Rudolph, D. L.. (1998). The dependence of the electrical conductivity measured by time domain reflectometry on the water content of a sand. *Water Resources Research*, Volume 34 (5), pp. 1207-1213.
- Ghazanfari, E.. (2013). Development of a mathematical model for electrically assisted oil transport in porous media.
- Ghazanfari, E., and Pamukcu, S.. (2014). Mathematical Modeling of Electrokinetic Transport and Enhanced Oil Recovery in Porous Geo-media. Chapter 5 in *Elektrokinetics for Petroleum and Environmental Engineers*, eds. Chilingar, G., and Haroun, M., John Wiley & Sons, Inc., New Jersey, and Scrivener Publishing, LLC, Massachusetts, pp. 177-236.
- Ghazanfari, E., Pamukcu, S., Pervizpour, M., and Karpyn, Z.. (2014). Investigation of Generalized Relative Permeability Coefficients for Electrically Assisted Oil Recovery in Oil Formations. *Journal of Transport in Porous Media*, Volume 105 (1), pp. 235-253.
- Ghyselbrecht, K., Huygebaert, M., Van der Bruggen, B., Ballet, R., Meesschaert, B., and Pinoy, L.. (2013). Desalination of an industrial saline water with conventional and bipolar membrane electrodialysis. *Desalination*, Volume 318, pp. 9-18.
- Godec, M., Van Leeuwen, T., and Kuuskraa, V.. (2007). Economics of Unconventional Gas. *OGJ Unconventional Gas*.
- Grattoni, C., and Dawe, R. A.. (1996). Electrical resistivity and fluid distribution of coexisting immiscible phases.
- Greenkorn, R. A.. (1983). Flow phenomena in porous media-Fundamentals and applications in petroleum, water and food production. New York (New York): Marcel Dekker Inc.
- Guo, K., Li, H., and Yu, Z.. (2016). In-situ heavy and extra heavy oil recovery: A review. *Fuel*, Volume 185, pp. 886-902.
- Haluszczak, L.O, Rose, A.W., and Kump, L.R.. (2012). Geochemical evaluation of flowback brine from Marcellus gas wells in Pennsylvania, USA. *Applied Geochemistry*.
- Handhal, A. M.. (2016). Prediction of reservoir permeability from porosity measurements for the upper sandstone member of Zubair Formation in Super-Giant South Rumila oil field, southern Iraq, using M5P decision trees and adaptive neuro-fuzzy inference system (ANFIS): a comparative study. *Modeling Earth Systems and Environment*, Volume 2 (111).
- Haroun, M. R., Chilingar, G.V., Pamukcu S., Wittle, K.J., and Al Boushi, M.N.. (2009). Optimizing electroosmotic flow potential for electrically enhanced oil recovery

- (EOR) in carbonate rock formations of Abu Dhabi based on rock properties and composition. Doha, Qatar.
- Hayes, T.. (2012). Barnett and Appalachian water management and reuse technologies. Research Partnership to Secure Energy for America (RPSEA) Report.
- Herman, R.. (2001). An introduction to electrical resistivity in geophysics. American Association of Physics Teachers.
- Hill, D.. (2014). Applications of Electro-Kinetics for Enhanced Oil Recovery. Chapter 3, in *Elektrokinetics for Petroleum and Environmental Engineers*, eds. Chilingar, G., and Haroun, M., John Wiley & Sons, Inc., NJ, and Scrivener Publishing, LLC, MA, pp. 33-102.
- Huang, C., Xu, T., Zhang, Y., Xue, Y., and Chen, G.. (2007). Application of electro dialysis to the production of organic acids: State of the art and recent developments. *Journal of Membrane Science*, Volume 288, pp. 1-12.
- Hunter, R.J.. (1981). *Zeta Potential in Colloid Science*. Academic Press, New York, NY.
- Islam, M. R., Mousavizadegan, S.H., Mustafiz, S., and Abou-Kassen, J.H.. (2010). *Advanced petroleum reservoir simulation*. Salem, MA: Scrivener Publishing LLC and John Wiley & Sons, Inc.
- Ju, B.. (2014). Mathematical model and analytical solutions for unsteady flow in natural gas reservoirs. *Journal of Porous Media*, Volume 17 (4), pp. 279-285.
- Kariduraganavar, M.Y., Nagarale, R.K., Kittur, A.A., and Kulkarni, S.S.. (2006). Ion-exchange membranes: preparative methods for electro dialysis and fuel cells applications. *Desalination*, Volume 197, pp. 225-246.
- Khaled, A.-R. A., and Vafai, K.. (2003). The role of porous media in modeling flow and heat transfer in biological tissues. *International Journal of heat and Mass Transfer*, Volume 46, pp. 4989-5003.
- Khatti, K.S.. (2007). Analyzing Finite Volume for Single-Phase Flow in Porous Media. *Journal of Porous Media*, Volume 10 (2), pp. 101 –123.
- Killough, L.E., and Gonzalez, J.A.. (1986). A fully implicit model for electrically enhanced oil recovery. In: *Proceedings of Society of Petroleum Engineering Conference*, New Orleans, LA.
- Kim, K.-Y., Han W. S., and Lee, P.-K.. (2014). Flow dynamics of CO<sub>2</sub>/brine at the interface between the storage formation and sealing units in a multi-layered model. *Transport in porous media*, Volume 105 (3), pp. 611-633.

- Korolev, V.A., Romanyukha, O.V., and Abyzova, A.M.. (2008). Electrokinetic remediation of oil-contaminated soils. *Journal of Environmental Science and Health, Part A Toxic / Hazardous Substances and Environmental Engineering*, Volume 43 (8), pp. 876-80.
- Latil, M.. (1980). *Enhanced oil recovery*. Gulf Publishing company.
- Lee, H.J., Sarfert, F., Strathmann, H., and Moon, S.H.. (2002). Designing of an electro dialysis desalination plant. *Desalination*, pp. 267-286.
- Li, K.. (2004). Theoretical development of the Brooks-Corey capillary pressure model from fractal modeling of porous media. *SPE/DOE Fourteenth Symposium on Improved Oil Recovery*, Tulsa, OK.
- Llorente, I., Fajardo, S., and Bastidas, J. M.. (2014). Application of electrokinetic phenomena in materials science. *Journal of State Electrochemistry*, Volume 18 (2), pp. 293-307.
- Lutz, B.D., Lewis, A.N., and Doyle, M.W.. (2013). Generation, transport, and disposal of wastewater associated with Marcellus Shale gas development. *Water Resources Research*, Volume 49, pp. 647-656.
- Maigrot, E., and Sabates, J.. (1890). *Apparat zur Lauterung von Zuckersaften mittels Elektrizitat*. Germ. Pat. Nr. 50443.
- Mohammadi, T., and Kaviani, A.. (2003). Water shortage and seawater desalination by electro dialysis. *Desalination*, Volume 158, pp. 267-270.
- Okandan, E.. (1984). *Heavy Crude Oil Recovery*. Hague: Martinus Nijhoff Publishers.
- Pamukcu, S., Filipova, I., and Wittle, J.K.. (1995). The Role of Electroosmosis in Transporting PAH Compounds in Contaminated Soils. *Electrochemical Technology Applied to Environmental Problems*, The Electrochemical Society, PV95-12, pp. 252-266.
- Pamukcu, S.. (2009). *Electrochemical Transport and Transformations*. Chapter 2. *Electrochemical Remediation Technologies for Polluted Soils, Sediments and Groundwater*, John Wiley & Sons, pg. 29.
- Pamukcu, S., Ghazanfari, E., and Wittle, J.K.. (2014). Reduction of Contaminants in Soil and Water by Direct Electric Current. Chapter 2, in *Electrokinetics for Petroleum and Environmental Engineers*, eds. Chilingar, G., and Haroun, M., John Wiley & Sons, Inc., New Jersey, and Scrivener Publishing, LLC, MA, pp. 33-102.
- Peraki, M., and Ghazanfari, E.. (2014). Electro dialysis treatment of flow-back water for environmental protection in shale gas development. *ASCE Shale Conference*, Pittsburgh, PA.

- Peraki, M., Ghazanfari, E., Pinder, G. F., and Harrington, T. L.. (2016). Electrodialysis: An application for the environmental protection in shale-gas extraction. *Separation and Purification Technology*, Volume 161, pp. 96-103.
- Peraki, M., Ghazanfari, E., and Pinder, G.F.. (2017). Numerical investigation of immiscible flow for waterflooding and electrically-enhanced oil recovery. *Transport in Porous Media*, Manuscript in review.
- Pilat, B.. (2001). Practice of water desalination by electrodialysis. *Desalination*, Volume 139, pp. 385-392.
- Pinder, G. F., and Gray, W. G.. (2008). *Essentials of multiphase flow and transport in porous media*. Hoboken, NJ: John Wiley & Sons, Inc.
- Rahm, B.G., Bates, JT., Bertoia, L.R., Galford, A.E., and Yoxtheimer, D.A.. (2013). Wastewater management and Marcellus Shale gas development: Trends, drivers, and planning implications. *Journal of Environmental Management*, Volume 120, pp. 105-113.
- Rajagopal, K., and Srinivasan, S.. (2014). Flow of fluids through porous media due to high pressure gradients: part 2 – unsteady flows. *Journal of Porous Media*, Volume 17, Issue 9, pages 751-762
- Ringen, J. K., Halvorsen, C., Lehne, K. A., Rueslaatten, H., and Holand, H.. (2001). Reservoir water saturation measured on cores; case histories and recommendations. 6th Nordic Symposium on Petrophysics, Trondheim, Norway.
- Sadikh-Zadeh, L.A.. (2006). Prediction of sandstone porosity through quantitative estimation of its mechanical compaction during lithogenesis (Bibieybat Field, South Caspian Basin). *Natural Resources Research*, Volume 15 (1), pp. 27-32.
- Sadrzadeh, M., Kaviani, A., and Mohammadi, T.. (2007). Mathematical modeling of desalination by electrodialysis. *Desalination*, Volume 206, pp. 538-546.
- Sadrzadeh, M., and Mohammadi, T.. (2008). Sea water desalination using electrodialysis. *Desalination*, Volume 221, pp. 440-447.
- Sadrzadeh, M., and Mohammadi, T.. (2009). Treatment of sea water using electrodialysis: Current efficiency evaluation. *Desalination*, Volume 249, pp. 279-285.
- Saichek, R.E., and Reddy, K.R.. (2005). Surfactant-enhanced Electrokinetic Remediation of Polycyclic Aromatic Hydrocarbons in Heterogeneous Subsurface Environments. *Journal of Environmental Engineering & Science*, Volume 4 (5), pp.327-339.
- Scheidegger, A. E.. (1957). *The physics of flow through porous media*. New York, NY: The Macmillan Company.

- Sheng, J. J.. (2014). Critical review of low-salinity waterflooding. *Journal of Petroleum Science and Engineering*, Volume 120, pp. 216-224.
- Shi, Y., Yang, Z., and Yang, D.. (2016). Determination of non-Darcy flow behavior in a tight formation. *Journal of Porous Media*, Volume 19 (8), pp. 687-700.
- Smoluchowski, M.. (1914). *Handbuch der Electricitat und des Magnetismus*, II (ed. Graetz, S.), J. A. Barth, Volume 2(336), Leipzig, Germany.
- Sonune, A., and Ghate, R.. (2004). Developments in wastewater treatment methods. *Desalination*, Volume 167, pp. 55-63.
- Strathmann, H.. (2010). Electrodialysis, a mature technology with a multitude of new applications. *Desalination*, Volume 264, pp. 268-288.
- Tanaka, Y.. (2012). Ion-exchange membrane electrodialysis program and its application to multi-stage continuous saline water desalination. *Desalination*, Volume 301, pp. 10-25.
- Tao, R., and Tang H.. (2014). Reducing viscosity of paraffin base crude oil with electric field for oil production and transportation. *Fuel*, Volume 118, pp. 69-72.
- Tchillingarian, G. V.. (1952). Possible utilization of electrokinetic phenomenon for separation of the fine sediments into grades. *Journal of Sedimentary Petrology*, Volume 22, pp. 29-32.
- Timur, A., Hemphins, W. B., and Worthington, A. E.. (1972). Porosity and pressure dependence of formation resistivity factor for sandstones. *Canadian Well Logging Society Transactions*, Volume 4.
- Turek, M.. (2002). Cost effective electrodialytic seawater desalination. *Desalination*, Volume 153, pp. 371-376.
- Veil, J.A.. (2010). *Water Management Technologies used by Marcellus Shale gas producers*. Argonne National Laboratory. Office of Fossil Energy, Argonne, IL.
- Wall, S.. (2010). The history of electrokinetic phenomena. *Current Opinion in Colloid and Interface Science*, Volume 15, pp. 119-124.
- Weir, G. J., White, S. P., and Kissling, W. M.. (1996). Reservoir storage and containment of greenhouse gases. *Transport in porous media*, Volume 23 (1), pp. 37-60.
- Winsauer, H. M.. (1952). Resistivity of brine-saturated sands in relation to pore geometry. *American Association of Petroleum Geologists Bulletin*, 36(2), pp. 253-277.
- Wise, D. L.. (2000). *Remediation engineering of contaminated soils.*: CRC Press.

- Wittle, J. K., and Hill, D. G.. (2006). Use of direct current electrical simulation for heavy oil production. Calgary, Canada, Society of Petroleum Engineers.
- Wittle, J.K., Hill, D.C., and Chilingar, G.V.. (2008). Direct Current Electrical Enhanced Oil Recovery in Heavy-Oil Reservoirs to Improve Recovery, Reduce Water Cut, and Reduce H<sub>2</sub>S Production while Increasing API Gravity. Society of Petroleum Engineers, SPE 114012.
- Wittle, J.K., Hill, D.G., and Chilingar, G.V.. (2011). Direct Electric Current Oil Recovery (EEOR) - A new approach to enhancing oil production. Energy Sources.
- Xu, T.. (2005). Ion exchange membranes: State of their development and perspective. Journal of Membrane Science, Volume 263, pp. 1-29.
- Ziemkiewicz, P., Hause, J., Lovett, R., Locke, D., Johnson, H., and Patchen, D.. (2012). Zero discharge water management for horizontal shale gas well development. Final report, West Virginia Water Research Institute and West Virginia University.

## APPENDIX A

### ELECTRODIALYSIS DATA FOR THE DILUTED CHAMBER

<b>Test</b>	<b>Initial concentration (mg/L)</b>	<b>Initial Conductivity (mS)</b>	<b>Final concentration (mg/L)</b>	<b>Final Conductivity (mS)</b>	<b>Change in TDS level (%)</b>	<b>Voltage (Volt)</b>
ED1-1	91780	80.2	104960	101.8	14.36	18.27
ED1-2	101035	103	91780	98.9	-9.16	9.00
ED1-3	93765	98.7	99515	100.1	6.13	17.31
ED1-4	101035	103	92520	76.6	-8.43	17.15
ED1-5	101035	103	109260	96.4	8.14	17.22
ED1-6	101035	103	94000	96.1	-6.96	17.30
ED1-7	101035	103	81230	87.8	-19.60	17.28
ED1-8	101305	105.5	75450	86.8	-25.52	17.25
ED1-9	101305	105.5	74350	86.3	-26.61	17.25
ED2-1	101035	103	93765	96.3	-7.20	9.00
ED2-2	101305	105.5	97200	99.2	-4.05	17.56
ED2-3	101305	105.5	99290	101.3	-1.99	17.07
ED2-4	94000	96.1	90280	89.1	-3.96	17.21
ED2-5	102585	106	95825	100	-6.59	15.46
ED2-6	102585	106	95260	99.8	-7.14	15.09
ED2-7	98370	101	97090	98.1	-1.30	17.19
ED2-8	102585	106.1	95295	100.2	-7.11	17.28
ED2-9	95295	100.6	92790	99.7	-2.63	17.39
ED3-1	68710	75.3	66140	74.9	-3.74	17.99
ED3-2	68710	75.3	66265	75	-3.56	17.94
ED3-3	66140	75.3	63180	74	-4.48	17.50
ED3-4	68710	75.3	66025	74.5	-3.91	17.90
ED3-5	66025	75.5	62645	73.7	-5.12	13.82
ED3-6	68710	75.3	64725	75	-5.80	15.85
ED3-7	68710	75.3	64170	72.5	-6.61	15.46
ED3-8	68710	75.3	67240	73	-2.14	15.46

ED3-9	68710	75.3	65195	74.2	-5.12	15.46
ED4-1	64130	75.3	57750	65.5	-9.95	17.33
ED4-2	64130	75.3	62345	73	-2.78	17.09
ED4-3	52470	65.4	48985	57.8	-6.64	17.36
ED4-4	64130	75.3	59700	69.2	-6.91	17.84
ED4-5	52470	65.4	47780	59.9	-8.94	17.34
ED4-6	52470	65.4	46290	61.9	-11.78	17.36
ED4-7	52470	65.4	51905	64.6	-1.08	17.35
ED4-8	52470	65.4	45925	58.3	-12.47	17.40
ED4-9	64130	75	51820	61.9	-19.20	17.39

## APPENDIX B

### ELECTRODIALYSIS DATA FOR THE CONCENTRATED CHAMBER

#### CLOSE TO THE ANODE

Test	Initial concentration (mg/L)	Final concentration (mg/L)	Change in TDS level (%)
ED1-1	102735	104840	2.05
ED1-2	101035	102735	1.68
ED1-3	89300	102415	14.69
ED1-4	101035	107860	6.76
ED1-5	101035	127995	26.68
ED1-6	101035	108250	7.14
ED1-7	101035	113920	12.75
ED1-8	101305	116685	15.18
ED1-9	101305	115080	13.60
ED2-1	101035	111625	10.48
ED2-2	101305	142393	40.56
ED2-3	101305	136413	34.66
ED2-4	108250	114635	5.90
ED2-5	102585	96090	-6.33
ED2-6	102585	96780	-5.66
ED2-7	98370	104795	6.53
ED2-8	102585	99575	-2.93
ED2-9	99575	95975	-3.62
ED3-1	68710	66890	-2.65
ED3-2	68710	69355	0.94
ED3-3	66890	64645	-3.36
ED3-4	68710	65580	-4.56
ED3-5	65580	65655	0.11
ED3-6	68710	65620	-4.50
ED3-7	68710	68545	-0.24
ED3-8	68710	67760	-1.38

ED3-9	68710	64235	-6.51
ED4-1	64130	70595	10.08
ED4-2	64130	67525	5.29
ED4-3	52470	56685	8.03
ED4-4	64130	71175	10.99
ED4-5	52470	58035	10.61
ED4-6	52470	59065	12.57
ED4-7	52470	66780	27.27
ED4-8	52470	60625	15.54
ED4-9	64130	76815	19.78

## APPENDIX C

### ELECTRODIALYSIS DATA FOR THE CONCENTRATED CHAMBER CLOSE TO THE CATHODE

Test	Initial concentration (mg/L)	Final concentration (mg/L)	Increase (%)
ED1-1	81820	104200	27.35
ED1-2	101035	81820	-19.02
ED1-3	98255	101870	3.68
ED1-4	101035	98895	-2.12
ED1-5	101035	113240	12.08
ED1-6	101035	101000	-0.03
ED1-7	101035	99125	-1.89
ED1-8	101305	95390	-5.84
ED1-9	101305	96620	-4.62
ED2-1	101035	98255	-2.75
ED2-2	101305	100570	-0.73
ED2-3	101305	101515	0.21
ED2-4	101000	103215	2.19
ED2-5	102585	97575	-4.88
ED2-6	102585	97980	-4.49
ED2-7	98370	100975	2.65
ED2-8	102585	97235	-5.22
ED2-9	97235	95180	-2.11
ED3-1	68710	66935	-2.58
ED3-2	68710	68705	-0.01
ED3-3	66935	65900	-1.55
ED3-4	68710	65775	-4.27
ED3-5	65775	65595	-0.27
ED3-6	68710	65010	-5.38
ED3-7	68710	67335	-2.00
ED3-8	68710	67270	-2.10
ED3-9	68710	65460	-4.73
ED4-1	64130	65165	1.61
ED4-2	64130	63720	-0.64
ED4-3	52470	54155	3.21

ED4-4	64130	64965	1.30
ED4-5	52470	54305	3.50
ED4-6	52470	54830	4.50
ED4-7	52470	60700	15.69
ED4-8	52470	53735	2.41
ED4-9	64130	63460	-1.04

## APPENDIX D

### MATLAB SCRIPT FOR NUMERICAL ANALYSIS OF EEOR

```
Dim.nx=60; Dim.ny=120; %number of cells in each axis
Dim.Lx=60; Dim.Ly=120; %length of reservoir in each axis [370, 670]
Dim.bx=Dim.Lx/Dim.nx; Dim.by=Dim.Ly/Dim.ny; %dimensions of control volumes
Dim.n=Dim.nx*Dim.ny;
Dim.vol=Dim.bx*Dim.by; %volume of each control volume

diagonal=sqrt(Dim.Lx^2+Dim.Ly^2); %distance between electrodes

%Properties of medium
Med.K=1e-14*ones(2,Dim.nx,Dim.ny); %absolute permeability [100 mD]
Med.phi=0.2*ones(Dim.nx,Dim.ny); %porosity
a=1.13; % cementation constant (0.35-4.78)
m=1.73; %cementation exponent (1.14-2.52)
Med.F=a./Med.phi.^m; %formation resistivity factor
Med.F=reshape(Med.F,Dim.n,1);

%sink/source term
q=zeros(Dim.n,1);
q(1)=0.009/85; %injection rate [5000bbl/85]

%Properties of the fluids
Mu.w=3e-4; Mu.o=2; %viscosities
Sirr.cw=0.2; Sirr.o=0.2; %irreducible saturations

%time parameters
nt=300; T=300*24*3600; dt=T/nt;
ntnt=zeros(nt+1,1);

% create pressure, Saturation, and production rate vectors

Sw=zeros(Dim.n,nt+1);%water saturation
So=zeros(Dim.n,nt+1);%oil saturation
P=zeros(Dim.n,nt);%pressure
Qprod=zeros(nt,1); %production rate
Qo=zeros(nt,1); %oil production rate

%Initial saturations
Sw(:,1)=Sirr.cw+0.2;
So(:,1)=1-Sw(:,1);
```

```
% electric properties
```

```
Rw=0.5; %[ohm m] resistivity of conate water  
n=2; %saturation exponent that depends on the type of rock (1-2.5)  
I_density=1; %current density [A/m^2]  
ke=1e-9; %[m^2/Volt sec] electroosmotic permeability
```

```
Resty=zeros(Dim.n,nt+1); %resistivity  
I=zeros(nt,1); %current [Amps]  
VG=zeros(nt,1); %voltage gradient [V/m]  
Power=zeros(nt,1); %applied power [kW]  
v=zeros(nt,1);  
Volt=zeros(Dim.n,nt);
```

```
[Resty(:,1),v(1),I(1),VG(1),resty,Power(1),psi,ker]=el_pr(Med.F,Sw(:,1),Rw,Dim,n,I_de  
nsity,diagonal,ke,Sirr);
```

```
fw_pr=zeros(nt+1,1);  
[kr]=relperm(Sw(:,1),Mu,Sirr);  
fw=kr.w./(kr.w+kr.o);  
fw_pr(1)=fw(Dim.n);
```

```
%%
```

```
h = waitbar(0,'Please wait...');
```

```
for t=1:nt
```

```
    t1=t*dt;
```

```
    Mu.o=2.635-(2.7e-7)*t1;
```

```
    [Volt(:,t)]=volt_distr(v(t),Dim);
```

```
    [V_el,G]=Qel_pr(Dim,psi,Volt(:,t));
```

```
    [P(:,t),V,Gamma,temp]=pressure(Dim,Med,q,Mu,Sirr,Sw(:,t));
```

```
    q(Dim.n)=temp*P(:,t)+G(Dim.n,:)*Volt(:,t);
```

```
    Qprod(t)=q(Dim.n);
```

```
    Qo(t)=(1-fw(Dim.n))*Qprod(t);
```

```
    [Sw(:,t+1),Ap,Ae,ntnt(t+1),fw]=satur(Dim,Med,Mu,Sirr,V,V_el,psi,q,dt,Sw(:,t));
```

```
    fw_pr(t+1)=fw(Dim.n);
```

```
    So(:,t+1)=1-Sw(:,t+1);
```

```
    [Resty(:,t+1),v(t+1),I(t+1),VG(t+1),resty,Power(t+1),psi,ker]=el_pr(Med.F,Sw(:,t+1),
```

```
    Rw,Dim,n,I_density,diagonal,ke,Sirr);
```

```
    waitbar(t/nt,h)
```

```
end
```

```
close(h)
```

## APPENDIX E

### MATLAB FUNCTIONS FOR NUMERICAL ANALYSIS OF EEOR

```
function [Resty,V,I,VG,resty,P,psi,ker] = el_pr(F,Sw,Rw,Dim,n,i,diagonal,ke,Sirr)
% Calculates the electric properties of the system
s_star=(Sw-Sirr.cw)/(1-Sirr.cw-Sirr.o);

Resty=zeros(Dim.n,1);

for m=1:Dim.n

    Resty(m)=F(m)*Rw/s_star(m)^n;

end

resty=mean(Resty); %mean resistivity of reservoir [ohm m]
VG=resty*i; %voltage gradient [V/m]
V=VG*diagonal; %voltage between electrodes [Volt]
I=V*2*pi*diagonal/resty; %current [Amps]
P=V*I/1000; %power [kW]

ker.ww=1.26.*s_star.^2.-0.19.*s_star+0.04; % relative electroosmotic permeability of
water phase with respect to the water phase
ker.wo=-0.52.*s_star.^2.+0.49.*s_star-0.03; % relative electroosmotic permeability of oil
phase with respect to the water phase

for i=1:Dim.n

    if ker.ww(i)>1
        ker.ww(i)=1;
    elseif ker.ww<0
        ker.ww=0;
    end

    if ker.wo(i)>1
        ker.wo(i)=1;
    elseif ker.wo<0
        ker.wo=0;
    end
end
end
```

```
psi.w=ke*ker.ww; %[m^2 V^-1 sec^-1]
psi.o=ke*ker.wo; %[m^2 V^-1 sec^-1]
```

```
end
```

```
function [A] =alphas(Dim,q,xf,yf)
%Generates the Alpha matrix for the determination of the saturation
```

```
q_out=min(q,0);
```

```
%negative and positive fluxes
```

```
xf.in=reshape(xf.in(2:Dim.nx+1,:),Dim.n,1); xf.out=reshape(xf.out(1:Dim.nx,:),Dim.n,1);
yf.in=reshape(yf.in(:,2:Dim.ny+1),Dim.n,1); yf.out=reshape(yf.out(:,1:Dim.ny),Dim.n,1);
```

```
Diagonals=[yf.in,xf.in,q_out-xf.in+xf.out-yf.in+yf.out,-xf.out,-yf.out];
Ind_diag=[-Dim.nx,-1,0,1,Dim.nx];
```

```
A=spdiags(Diagonals,Ind_diag,Dim.n,Dim.n);
```

```
end
```

```
function [P,V,Gamma,temp] = pressure(Dim,Med,q,Mu,Sirr,Sw)
%Calculates pressure distribution using the Two Point Flux Approximation
%method
```

```
[kr]=relperm(Sw,Mu,Sirr);
kr.tot=kr.w+kr.o;
```

```
lambda=reshape([kr.tot,kr.tot]',2,Dim.nx,Dim.ny).*Med.K;
```

```
%pressure solver + fluxes
```

```
[P,V,Gamma,temp]=TPFA(Dim,lambda,q);
```

```
end
```

```

function [kr] = relperm(Sw,Mu,Sirr)

%calculate mobility

lambda=4; %coefficient Brooks and Corey (1964)

s_star=(Sw-Sirr.cw)/(1-Sirr.cw-Sirr.o);
kr.w=s_star.^((2+3*lambda)/lambda)/Mu.w; %relative permeability of water/viscosity of
water
kr.o=(1-s_star.^((2+lambda)/lambda)-
2.*s_star+2.*s_star.^((2+lambda)/lambda+1)+s_star.^2-
s_star.^((2+lambda)/lambda+2))/Mu.o; %relative permeability of oil/viscosity of oil

end

function [Sw,Alphap,Alphae,nt,fw] =satur(Dim,Med,Mu,Sirr,V,V_el,psi,q,dt,Sw)
%Calculates saturation using explicit method

pv=Dim.vol(:).*Med.phi; %pore volume

Psi=psi.w;
% Psi=reshape([Psi,Psi]',2,Dim.nx,Dim.ny);

q_in=max(q,0); %inflow from well
q_in=reshape(q_in,Dim.nx,Dim.ny);
%positive and negative fluxes in all axes

%pressure
xfp.in=max(V.x,0); xfp.out=min(V.x,0);
yfp.in=max(V.y,0); yfp.out=min(V.y,0);

ftot.p=xfp.in(1:Dim.nx,:)+yfp.in(:,1:Dim.ny)-xfp.out(2:Dim.nx+1,:)-
yfp.out(:,2:Dim.ny+1);

%electric field

xfe.in=max(V_el.x,0); xfe.out=min(V_el.x,0);
yfe.in=max(V_el.y,0); yfe.out=min(V_el.y,0);

ftot.e=xfe.in(1:Dim.nx,:)+yfe.in(:,1:Dim.ny)-xfe.out(2:Dim.nx+1,:)-
yfe.out(:,2:Dim.ny+1);

ftotal=ftot.p+ftot.e;

```

```
%stability for explicit method
```

```
influx=min(pv./(ftotal+q_in));  
cfl=((1-Sirr.cw-Sirr.o)/3).*influx;  
nt=ceil(dt./cfl);  
nt=max(nt);  
dtdt=(dt/nt)./pv;  
dtdt=reshape(dtdt,Dim.n,1);  
Ap=alphas(Dim,q,xfp,yfp);  
Ae=alphas(Dim,q,xfe,yfe);
```

```
Alphap=spdiags(dtdt,0,Dim.n,Dim.n)*Ap;  
Alphae=spdiags(dtdt,0,Dim.n,Dim.n)*Ae;  
q_in=max(q,0).*dtdt;
```

```
for t=1:nt
```

```
    [kr]=relperm(Sw,Mu,Sirr);
```

```
    fw=kr.w./(kr.w+kr.o);
```

```
    Sw=Sw+Alphap*fw+q_in+Alphae*Psi;
```

```
end
```

```
for i=1:Dim.n
```

```
    if Sw(i)>0.8
```

```
        disp('Saturation greater than 0.8')
```

```
    elseif Sw(i)<0.2
```

```
        disp('Saturation less than 0.2')
```

```
    end
```

```
end
```

```
end
```

```

function [p,V,Gamma,temp] =TPFA(Dim,lambda,q)

%calculates pressure distribution and extract fluxes

L=lambda.^(-1);

%transmissibilities in all axes (harmonic average)
tr.x=2*Dim.by/Dim.bx;
tr.y=2*Dim.bx/Dim.by;
Trans.x=zeros(Dim.nx+1,Dim.ny); Trans.x(2:Dim.nx,:)=tr.x./(L(1,1:Dim.nx-
1,.)+L(1,2:Dim.nx,:));
Trans.y=zeros(Dim.nx,Dim.ny+1); Trans.y(:,2:Dim.ny)=tr.y./(L(2,:,1:Dim.ny-
1)+L(2,:,2:Dim.ny));

%Assembly of Matrix
x1=reshape(Trans.x(1:Dim.nx,:),Dim.n,1);
x2=reshape(Trans.x(2:Dim.nx+1,:),Dim.n,1);
y1=reshape(Trans.y(:,1:Dim.ny),Dim.n,1);
y2=reshape(Trans.y(:,2:Dim.ny+1),Dim.n,1);

Diagonals=[-y2,-x2,x1+x2+y1+y2,-x1,-y1];
Ind_diag=[-Dim.nx,-1,0,1,Dim.nx];
Gamma=spdiags(Diagonals,Ind_diag,Dim.n,Dim.n);
temp=Gamma(Dim.n,:);
Gamma(Dim.n,:)=0;
Gamma(Dim.n,Dim.n)=1;
q(Dim.n)=27579029.2;

p=Gamma\q;
%pressure
P=reshape(p,Dim.nx,Dim.ny);
%flux in each axis
V.x=zeros(Dim.nx+1,Dim.ny);
V.y=zeros(Dim.nx,Dim.ny+1);
V.x(2:Dim.nx,:)=(P(1:Dim.nx-1,:)-P(2:Dim.nx,:)).*Trans.x(2:Dim.nx,:);
V.y(:,2:Dim.ny)=(P(:,1:Dim.ny-1)-P(:,2:Dim.ny)).*Trans.y(:,2:Dim.ny);
end

function [G,V_el] =TPFA_electrical(Dim,psi,Volt)

```

```
%calculates pressure distribution and extract fluxes
```

```
L=psi.^(-1);
```

```
%transmissibilities in all axes (harmonic average)
```

```
tr.x=2*Dim.by/Dim.bx;
```

```
tr.y=2*Dim.bx/Dim.by;
```

```
Trans.x=zeros(Dim.nx+1,Dim.ny); Trans.x(2:Dim.nx,:)=tr.x./(L(1,1:Dim.nx-1,)+L(1,2:Dim.nx,:));
```

```
Trans.y=zeros(Dim.nx,Dim.ny+1); Trans.y(:,2:Dim.ny)=tr.y./(L(2,:,1:Dim.ny-1)+L(2,:,2:Dim.ny));
```

```
%Assembly of Matrix
```

```
x1=reshape(Trans.x(1:Dim.nx,:),Dim.n,1);
```

```
x2=reshape(Trans.x(2:Dim.nx+1,:),Dim.n,1);
```

```
y1=reshape(Trans.y(:,1:Dim.ny),Dim.n,1);
```

```
y2=reshape(Trans.y(:,2:Dim.ny+1),Dim.n,1);
```

```
Diagonals=[-y2,-x2,x1+x2+y1+y2,-x1,-y1];
```

```
Ind_diag=[-Dim.nx,-1,0,1,Dim.nx];
```

```
G=spdiags(Diagonals,Ind_diag,Dim.n,Dim.n);
```

```
volt=reshape(Volt,Dim.nx,Dim.ny);
```

```
%flux in each axis
```

```
V_el.x=zeros(Dim.nx+1,Dim.ny);
```

```
V_el.y=zeros(Dim.nx,Dim.ny+1);
```

```
V_el.x(2:Dim.nx,:)=(volt(1:Dim.nx-1,:)-volt(2:Dim.nx,:)).*Trans.x(2:Dim.nx,:);
```

```
V_el.y(:,2:Dim.ny)=(volt(:,1:Dim.ny-1)-volt(:,2:Dim.ny)).*Trans.y(:,2:Dim.ny);
```

```
end
```